



Gap solitons and their linear stability in one-dimensional periodic media

Guenbo Hwang^a, T.R. Akylas^b, Jianke Yang^{a,*}

^a Department of Mathematics and Statistics, University of Vermont, Burlington, VT 05401, USA

^b Department of Mechanical Engineering, Massachusetts Institute of Technology, Cambridge, MA 02139, USA

ARTICLE INFO

Article history:

Received 7 December 2010

Accepted 8 March 2011

Available online 16 March 2011

Communicated by J. Bronski

Keywords:

Gap solitons

Linear stability

Periodic potential

Exponential asymptotics method

ABSTRACT

An analytical theory utilizing exponential asymptotics is presented for one-dimensional gap solitons that bifurcate from edges of Bloch bands in the presence of a *general* periodic potential. It is shown that two soliton families bifurcate out from every Bloch-band edge under self-focusing or self-defocusing nonlinearity, and an asymptotic expression for the eigenvalues associated with the linear stability of these solitons is derived. The locations of these solitons relative to the underlying potential are determined from a certain recurrence relation, that contains information beyond all orders of the usual perturbation expansion in powers of the soliton amplitude. Moreover, this same recurrence relation decides which of the two soliton families is unstable. The analytical predictions for the stability eigenvalues are in excellent agreement with numerical results.

© 2011 Elsevier B.V. All rights reserved.

1. Introduction

Nonlinear wave propagation in periodic media is a fascinating subject that is currently at the forefront of research in optics, Bose–Einstein condensates and applied mathematics [1–6]. Due to periodicity of the media, the linear wave spectrum features Bloch bands and bandgaps. In addition, the curvature of the dispersion (or diffraction) surface can be positive as well as negative at different band edges, implying that wave localization can occur under either self-focusing or self-defocusing nonlinearity. This wave localization leads to the formation of static solitary waves, often referred to as gap solitons, inside the bandgaps of the periodic media. So far, a wide variety of gap solitons have been reported both theoretically and experimentally in *symmetric* (mostly sinusoidal) periodic potentials. These solitons can be divided into two groups, depending on whether or not they bifurcate from edges of Bloch bands. In one dimension (1D), two families of gap solitons, namely on-site and off-site solitons, bifurcate out from every edge of a Bloch band under self-focusing or self-defocusing nonlinearity [6–11]. On-site solitons are the ones whose centers are located at the minima of the sinusoidal potential (these minima are often called lattice sites), while off-site solitons are the ones whose centers are located halfway between lattice sites. In two dimensions (2D), at least four families of gap solitons, one on-site and the other three off-site, bifurcate out from every edge of a Bloch band under self-focusing or self-defocusing nonlinearity [12–16]. Moreover, there also exist many other gap solitons which do

not bifurcate from band edges. Notable examples include vortex solitons [17–24], truncated-Bloch-wave solitons [25–27], certain types of dipole solitons [6,9,28], and most arbitrary-shaped solitons [6]. Since these solitons do not bifurcate from band edges, their power curves exhibit multiple branches [6,23,27,28].

The stability of gap solitons is an important issue that has also attracted attention in recent years. In 1D, the linear stability of gap solitons that bifurcate from band edges was analyzed in [10]. Specifically, an analytical formula was derived for a small eigenvalue that bifurcates out from zero when a gap soliton bifurcates out from a band edge. According to this formula, near band edges in a symmetric sinusoidal potential, on-site solitons are linearly stable, while off-site solitons are linearly unstable, in qualitative agreement with numerical results. In addition, this formula reveals that the unstable eigenvalue is exponentially small with respect to the soliton amplitude. However, no quantitative comparison of the analytical eigenvalue expression against numerical results was made in [10].

In 2D, the linear stability of gap solitons that bifurcate from band edges in symmetric sinusoidal potentials was investigated in [29]. Through asymptotic calculations, an analytical formula was derived for a small eigenvalue which bifurcates out from zero when the gap soliton bifurcates out from a band edge (this eigenvalue has no counterpart in 1D). It turns out that this eigenvalue is unstable if the slope of the power curve has the opposite sign of nonlinearity (the self-focusing nonlinearity is said to have positive sign, and self-defocusing nonlinearity to have negative sign). This result generalizes the classical Vakhitov–Kolokolov stability criterion to sign-indefinite solitons [2,6,30], and brings out the critical role that the sign of nonlinearity plays in the stability of gap solitons in general. Quantitatively, the eigenvalue formula derived in [29] reveals that

* Corresponding author.

E-mail address: jyang@cems.uvm.edu (J. Yang).

the instability growth rate in 2D is algebraically small, rather than exponentially small, with respect to the soliton amplitude. Numerical computations [29] of power curves indicate that the slope of the power curve near band edges always has the opposite sign of nonlinearity, thus all 2D gap solitons near band edges are linearly unstable. Detailed quantitative comparison between the analytical eigenvalue formula and numerical eigenvalues was also performed in [29], and excellent agreement was obtained; hence the analytical eigenvalue formula for two dimensions was fully confirmed. Away from band edges, on-site 2D solitons could become stable, but off-site 2D solitons remain unstable due to additional symmetry-breaking instabilities [29].

In this paper, we revisit the problem of 1D gap solitons that bifurcate from band edges, and their linear stability properties, in a periodic potential. The original motivation for this work comes from the fact that the previous analytical calculation of the stability eigenvalues of gap solitons near band edges [10] is flawed. Specifically, in that work, the eigenvalue was given in terms of the derivative of the Melnikov function $M(x_0) \equiv \int_{-\infty}^{\infty} V'(x)\psi^2(x)dx$, where $V(x)$ is the periodic potential, and x_0 is the position of the peak of the envelope of Bloch-wave packet solution $\psi(x)$. The Melnikov function was then approximated using for $\psi(x)$ the leading-order term of the usual perturbation expansion in powers of the soliton amplitude ϵ near the band edge. However, it is straightforward to check that all higher-order terms in the perturbation series of $\psi(x)$ make contributions to $M(x_0)$ which are of the same order of magnitude in ϵ as the first term used for the eigenvalue formula presented in [10]. Consequently, ignoring these additional contributions not only would yield quantitatively inaccurate results for the stability eigenvalues, but also could conceivably alter the signs of these eigenvalues, thus leading to an erroneous stability result. One might potentially salvage the stability analysis in [10] by attempting to sum up the contributions to $M(x_0)$ from all higher-order terms in the perturbation expansion of $\psi(x)$, but the algebra involved seems formidable.

Apart from handling the difficulty mentioned above, the main goal of the present study is to provide a theoretical analysis for gap solitons and their stability in a *general* periodic potential. In all previous studies, the periodic potential was assumed to be symmetric (and mostly sinusoidal) [6,9,10,27]. In those special cases, the locations of gap solitons relative to the underlying potential are easy to obtain (see [6,10] and later text), but there is no simple criterion for determining these locations when the potential is no longer symmetric. In addition, there is recent interest in time-dependent periodic potentials [31] and aperiodic potentials [32,33], and our effort may serve as a natural bridge to studying nonlinear wave phenomena in those more general settings.

In the present paper, we develop an analytical method for determining the positions of 1D gap solitons and their linear-stability eigenvalues near band edges in the presence of a general periodic potential. For this purpose, in line with numerical evidence that the stability eigenvalues near band edges are exponentially small with respect to the soliton amplitude (as was realized in [10]), we utilize techniques of exponential asymptotics. The approach taken here parallels that in [34,35] for determining the envelope positions and linear stability properties of elevation and depression waves in the fifth-order KdV equation. We shall show that, in the presence of general periodic potentials, two families of gap solitons also bifurcate out from every Bloch-band edge under self-focusing or self-defocusing nonlinearity. However, the locations of these solitons relative to the underlying potential need to be determined from a certain recurrence relation, which contains information beyond all orders of the usual perturbation expansion in powers of the soliton amplitude. Moreover, based on this recurrence relation, we shall derive an asymptotic formula

for the linear-stability eigenvalues. These eigenvalues are indeed exponentially small. In addition, one of the two soliton families is always stable and the other one unstable. Quantitative comparison between this eigenvalue formula and numerical results is also performed, and excellent agreement is obtained.

As mentioned earlier, our theoretical approach follows along the lines of the exponential asymptotics technique in the wavenumber domain developed in [34,35] for the study of solitary wave packets in the fifth-order KdV equation. However, in the earlier work, some subtle issues were not addressed, especially regarding the validity of the solution to an integral equation, which plays an important part in this exponential asymptotics procedure. Interestingly enough, the same integral equation appears in our exponential asymptotics calculation for gap solitons as well, and we shall show that the solution to this integral equation given in [34] is valid only in certain regions of the complex plane. This finding has important consequences when one performs the inverse Fourier transform to obtain the physical solution. In addition, the approach taken here bypasses certain nontrivial calculations of [34], thus simplifying and streamlining the overall theoretical treatment.

2. Bloch-wave packets near band edges

We study the nonlinear Schrödinger equation with a general periodic potential $V(x)$,

$$i\Psi_t + \Psi_{xx} - V(x)\Psi + \sigma|\Psi|^2\Psi = 0, \quad (2.1)$$

where $\sigma = \pm 1$ denotes the sign of nonlinearity; when $\sigma = 1$, the nonlinearity is self-focusing, and when $\sigma = -1$, the nonlinearity is self-defocusing. In addition, the period of the potential $V(x)$ is taken to be equal to π without any loss of generality.

Solitary waves in Eq. (2.1) are sought in the form

$$\Psi(x, t) = \psi(x)e^{-i\mu t}, \quad (2.2)$$

where μ is the propagation constant, and the amplitude function $\psi(x)$ is real-valued and solves the ordinary differential equation

$$\psi_{xx} - V(x)\psi + \mu\psi + \sigma\psi^3 = 0. \quad (2.3)$$

When $\psi(x)$ is infinitesimal, Eq. (2.3) reduces to the linear Schrödinger equation

$$\psi_{xx} - V(x)\psi + \mu\psi = 0. \quad (2.4)$$

By the Bloch–Floquet theorem, solutions to this linear equation can be sought in the form of Bloch modes

$$p(x; \mu) = e^{ikx}\tilde{p}(x; \mu), \quad (2.5)$$

where $\tilde{p}(x; \mu)$ is periodic with the same period π as the potential $V(x)$, $\mu = \mu(k)$ is the dispersion relation, and $-1 \leq k \leq 1$ is the first Brillouin zone. The values of $\mu(k)$ form Bloch bands, where k is real and the Bloch modes (2.5) propagate, and these bands are separated by stop bands, or gaps, where k turns out to be complex, implying evanescent behavior. At a band edge μ_0 , $k = 0$ or ± 1 , thus the Bloch mode $p(x; \mu_0)$ is periodic with period π or 2π [5]. In addition, $p(x; \mu_0)$ is real-valued.

When $\psi(x)$ is not infinitesimal, solitary waves can bifurcate out from band edges into bandgaps, and these waves are called gap solitons in the literature. Near band edges, gap solitons are low-amplitude slowly varying Bloch-wave packets and can be determined by the multiscale perturbation method. Specifically, we expand $\psi(x)$ into a multiscale perturbation series,

$$\psi = \epsilon\psi_0 + \epsilon^2\psi_1 + \epsilon^3\psi_2 + \dots, \quad (2.6)$$

$$\mu = \mu_0 + \eta\epsilon^2, \quad (2.7)$$

where

$$\psi_0 = A(X)p(x) \quad (2.8)$$

is a Bloch-wave packet, $p(x) \equiv p(x; \mu_0)$ is the Bloch wave at edge μ_0 , $\eta = \pm 1$, $\epsilon \ll 1$, and $X = \epsilon x$ is the slow variable of the envelope function $A(X)$. Notice that ϵ^2 is the distance between the propagation constant μ and the band edge μ_0 , and ϵ also is an amplitude parameter of the gap soliton.

Substituting the above expansions into Eq. (2.3) and solving the resulting linear equations for ψ_n , we obtain [5,10]

$$\psi(x; X) = \epsilon A(X)p(x) + \epsilon^2 A'(X)v(x) + \dots, \quad (2.9)$$

where $v(x)$ is a generalized Bloch function and solves

$$v_{xx} + [\mu_0 - V(x)]v = -2p_x, \quad (2.10)$$

and the envelope function $A(X)$ satisfies the steady NLS equation

$$D \frac{d^2 A}{dX^2} + \eta A + \sigma \alpha A^3 = 0, \quad (2.11)$$

with

$$D = \frac{1}{2} \frac{d^2 \mu}{dk^2} \Big|_{\mu=\mu_0}, \quad \alpha = \frac{\int_0^{2\pi} p^4(x) dx}{\int_0^{2\pi} p^2(x) dx} > 0. \quad (2.12)$$

It is noted that since $p(x)$ is a homogeneous solution of (2.10), the solution $v(x)$ to the inhomogeneous equation (2.10) is not unique, and one may add a term $\zeta p(x)$, where ζ is a free constant. Returning to the expansion (2.9), we can see that adding $\zeta p(x)$ to $v(x)$ amounts to a shift in the position of the envelope $A(X)$. In order to fix the location of the envelope $A(X)$, we require that $v(x)$ be orthogonal to $p(x)$,

$$\int_0^{2\pi} p(x)v(x) dx = 0. \quad (2.13)$$

This orthogonality requirement uniquely determines the solution $v(x)$. If the potential $V(x)$ is symmetric, then $p(x)$ is either symmetric or antisymmetric. In this case, $v(x)$ would have the opposite symmetry of $p(x)$ under the above orthogonality condition.

When $\text{sgn}(\sigma) = \text{sgn}(D) = -\text{sgn}(\eta)$, the soliton solution of the envelope Eq. (2.11) is

$$A(X) = a \operatorname{sech} \frac{X - X_0}{\beta}, \quad (2.14)$$

where

$$a = \sqrt{2/\alpha}, \quad \beta = \sqrt{|D|}, \quad (2.15)$$

and $X_0 = \epsilon x_0$ is the position of the peak of the soliton's envelope $A(X)$. Below we shall refer to x_0 as the position of the soliton. Since the envelope Eq. (2.11) is translation-invariant, $A(X)$ would be a solution of this equation for any value of the parameter x_0 . Note also that, since $\text{sgn}(D) = -\text{sgn}(\eta)$, it follows from Eq. (2.7) and the definition of D in (2.12) that the propagation constant μ always lies inside the bandgap, thus the resulting soliton is always a gap soliton.

Pursuing the above perturbation expansion to higher orders, it is straightforward to show that, for any soliton position x_0 , a localized solution ψ_n ($n \geq 2$) in Eq. (2.6) can always be found. This seems to suggest that gap solitons of Eq. (2.3) can be located at arbitrary positions x_0 relative to the underlying potential. However, as the periodic potential in Eq. (2.3) breaks the translational invariance, it would appear unlikely that the gap soliton can be freely placed regardless of the periodic potential. This suspicion turns out to be correct. Indeed, it was realized in [10]

that a true gap soliton $\psi(x; x_0)$ in Eq. (2.3), with x_0 being the soliton's position, must also satisfy

$$M(x_0) \equiv \int_{-\infty}^{\infty} V'(x)\psi^2(x; x_0) dx = 0, \quad (2.16)$$

where $M(x_0)$ was called the Melnikov function in [10]. This constraint can be readily obtained by multiplying Eq. (2.3) with ψ_x and then integrating with respect to x . Inserting the perturbation series (2.9) into (2.16), one can see that $M(x_0)$ is exponentially small in ϵ , thus this constraint is not visible in the above perturbation series solution.

Approximating the perturbation series solution (2.9) by its leading-order term $\epsilon \psi_0$ in the Melnikov integral, it was concluded in [10] that the constraint (2.16) could only be satisfied for two values of x_0 in each period of the potential $V(x)$. For the $\sin^2 x$ potential, in particular, x_0 is either 0 or $\pi/2$, corresponding to on-site and off-site solitons, respectively. However, what was not realized in [10] is that all higher-order terms in the perturbation series (2.9) make contributions of the same order of magnitude in ϵ to the Melnikov function $M(x_0)$ —a fact which can be readily verified by straightforward calculations. For symmetric π -periodic potentials, all contributions to the Melnikov integral in (2.16) from the perturbation series (2.9) happen to be zero when $x_0 = 0$ or $\pi/2$; hence, the constraint (2.16) is indeed satisfied at these two x_0 positions [6]. On the other hand, for periodic potentials that are not symmetric, computing the Melnikov function $M(x_0)$ based on the leading-order term $\epsilon \psi_0$ for ψ alone would give the wrong locations x_0 of gap solitons. If one attempts to collect contributions to the Melnikov function $M(x_0)$ from all higher-order terms in the perturbation series (2.9), the algebra involved quickly becomes formidable. In view of these difficulties, we shall develop a different analytical method to calculate the locations of gap solitons that is applicable not only for symmetric periodic potentials but also for general periodic potentials. It will be shown that locations of these solitons, in general, are determined from a certain recurrence relation that contains information beyond all orders of the perturbation expansion in powers of ϵ .

3. Growing tails of exponentially small amplitude

In this section, we consider the stationary NLS Eq. (2.3) with a general π -periodic potential, and show that true gap solitons exist only at two locations x_0 which are determined from a certain recurrence relation. Our strategy is to examine solutions of Eq. (2.3) which are decaying at $x \rightarrow -\infty$ (upstream), and show that these solutions would develop growing tails with amplitude proportional to $\sin(2x_0 - \theta)$ for $x \gg 1/\epsilon$ (downstream), where θ is a constant which will be specified. It would then become obvious that these solutions are localized (i.e., are true gap solitons) only when $x_0 = \theta/2$ and $(\theta + \pi)/2$, and are nonlocal for all other values of x_0 . These growing tails turn out to be exponentially small in ϵ , consistent with the fact that they are not present in the perturbation series solution (2.9) at any power of ϵ . Calculation of these exponentially small, but growing, tails is crucial not only for determining the positions of gap solitons, but also for computing the linear-stability eigenvalues of gap solitons (see Section 4). The approach taken here is based on the exponential asymptotics technique in the wavenumber domain developed in [34] for computing the growing tails of solitary wave-packet solutions of the fifth-order KdV equation. Along the way, we will also clarify some subtle issues in this exponential asymptotics method and simplify its steps.

Let $\psi(x, X)$ be the perturbation series solution of Eq. (2.3) given by Eq. (2.9). We require that this solution be decaying upstream

($x \rightarrow -\infty$). Then, from the leading-order term in (2.9), the upstream asymptotic behavior is

$$\psi \sim 2\epsilon a e^{(x-x_0)/\beta} p(x), \quad x \rightarrow -\infty. \quad (3.1)$$

We will show that this solution downstream ($x \gg 1/\epsilon$) develops growing tails of exponentially small amplitude, and the downstream asymptotic behavior takes the form

$$\psi \sim 2\epsilon a e^{-(x-x_0)/\beta} p(x) + H e^{(x-x_0)/\beta} p(x), \quad x \gg 1/\epsilon. \quad (3.2)$$

Here $H(\epsilon, x_0)$ denotes the amplitude of the growing tail, which is exponentially small in ϵ , and it vanishes at two locations x_0 where gap solitons result (the expression for H will be given in Eq. (3.41)). The reason for the presence of this growing tail is that when $\psi \ll 1$, the nonlinear equation (2.3) reduces to the linear equation (2.4) with periodic coefficients. Since μ lies inside the bandgap, according to Bloch–Floquet theory, Eq. (2.4) has two linearly independent solutions, one proportional to $e^{-x/\beta} p(x)$, and the other one proportional to $e^{x/\beta} p(x)$. If we demand the solution to the nonlinear Eq. (2.3) to contain only the decaying mode $e^{-x/\beta} p(x)$ upstream ($x \rightarrow -\infty$), then the solution downstream ($x \gg 1/\epsilon$) would, in general, comprise both the decaying mode $e^{-x/\beta} p(x)$ and the growing mode $e^{x/\beta} p(x)$ as indicated in (3.2). The calculation of the amplitude H of the growing tail in (3.2) is the key step of the present study.

To this end, we first introduce the Fourier transform of the solution $\psi(x, X)$ with respect to the slow variable X ,

$$\widehat{\psi}(x, K) = \frac{1}{2\pi} \int_{-\infty}^{\infty} \psi(x, X) e^{-iKX} dX. \quad (3.3)$$

Since we anticipate an exponentially growing tail of the form (3.2) in the solution $\psi(x, X)$, this Fourier transform should not be taken for real wavenumbers K (where the integral in (3.3) does not converge). Instead, K should be complex with imaginary part equal to $-1/\beta$, so that the integrand in (3.3) is bounded as $X \rightarrow \pm\infty$. We shall come back to this point later in this section.

Inserting the perturbation series solution (2.9) into the Fourier transform (3.3), we get

$$\widehat{\psi}(x, K) = \frac{a\beta}{2} \epsilon e^{-iKx_0} \operatorname{sech}\left(\frac{\pi}{2}\beta K\right) [p(x) + i\epsilon K v(x) + \dots]. \quad (3.4)$$

The perturbation series (3.4) in the wavenumber domain is disordered when $\kappa \equiv \epsilon K = O(1)$, thus it is replaced by the uniformly valid expression

$$\widehat{\psi}(x, K) = \epsilon e^{-iKx_0} \operatorname{sech}\left(\frac{\pi}{2}\beta K\right) U(x, \kappa), \quad (3.5)$$

where

$$U(x, \kappa) = \frac{a\beta}{2} [p(x) + i\kappa v(x) + \dots] \quad (\kappa \ll 1). \quad (3.6)$$

Below, we will show that the function $U(x, \kappa)$ has simple-pole singularities of exponentially small residue at $\kappa \approx \pm 2$; these singularities then lead to a growing tail of exponentially small amplitude in the physical domain. Thus the main goal is to determine the local behavior of $U(x, \kappa)$ near these singularities.

We now derive the equation governing the function $U(x, \kappa)$. Inserting the two-scale solution $\psi(x, X)$ into Eq. (2.3), we get

$$\psi_{xx} + 2\epsilon \psi_{xX} + \epsilon^2 \psi_{XX} - V(x)\psi + \mu\psi + \sigma\psi^3 = 0. \quad (3.7)$$

Here the derivative to x is with respect to the fast variable x in ψ only. Taking the Fourier transform of this equation with respect to the slow variable X (as in (3.3)), the transformed equation for $\widehat{\psi}(x, K)$ is

$$\widehat{\psi}_{xx} + 2i\kappa \widehat{\psi}_x + [\mu - \kappa^2 - V(x)]\widehat{\psi} + \sigma \widehat{\psi}^3 = 0. \quad (3.8)$$

Substituting the expression (3.5) into this equation, we find that $U(x, \kappa)$ satisfies the equation

$$U_{xx} + 2i\kappa U_x + [\mu - \kappa^2 - V(x)]U + \sigma \cosh \frac{\pi\beta\kappa}{2\epsilon} \times \int_{-\infty}^{\infty} d\lambda \frac{U(x, \kappa - \lambda)}{\cosh \frac{\pi\beta(\kappa-\lambda)}{2\epsilon}} \int_{-\infty}^{\infty} d\rho \frac{U(x, \lambda - \rho)U(x, \rho)}{\cosh \frac{\pi\beta(\lambda-\rho)}{2\epsilon} \cosh \frac{\pi\beta\rho}{2\epsilon}} = 0. \quad (3.9)$$

This integral equation for $U(x, \kappa)$ is central to the ensuing analysis.

3.1. The recurrence relation

We first focus on $U(x, \kappa)$ for $\kappa = O(1)$, but away from possible singularities (i.e., $-2 < \kappa < 2$, since the dominant singularities will be shown to appear at $\kappa \approx \pm 2$). In the limit of $\epsilon \rightarrow 0$, the main contribution to the double integral in Eq. (3.9) then comes from the region of $0 < \lambda < \kappa, 0 < \rho < \lambda$ when $\kappa > 0$ and $\kappa < \lambda < 0, \lambda < \rho < 0$ when $\kappa < 0$; otherwise the integral is exponentially small in ϵ due to the hyperbolic functions. In these regions,

$$\cosh \frac{\pi\beta(\lambda - \rho)}{2\epsilon} \cosh \frac{\pi\beta\rho}{2\epsilon} \approx \frac{1}{2} \cosh \frac{\pi\beta\lambda}{2\epsilon}, \quad (3.10a)$$

$$\cosh \frac{\pi\beta(\kappa - \lambda)}{2\epsilon} \cosh \frac{\pi\beta\lambda}{2\epsilon} \approx \frac{1}{2} \cosh \frac{\pi\beta\kappa}{2\epsilon}, \quad (3.10b)$$

thus the integral equation (3.9) reduces to

$$U_{xx} + 2i\kappa U_x + [\mu - \kappa^2 - V(x)]U + 4\sigma \times \int_0^\kappa d\lambda U(x, \kappa - \lambda) \int_0^\lambda d\rho U(x, \lambda - \rho)U(x, \rho) = 0. \quad (3.11)$$

The difference between this simplified integral equation and (3.9) is exponentially small in ϵ . Thus the solution $U(x, \kappa)$ to this reduced Eq. (3.11), when combined with Eq. (3.5), furnishes precisely the Fourier transform of the power series solution (2.9). However, Eq. (3.11) is not easy to solve since its solution $U(x, \kappa)$ also depends on ϵ due to the relation $\mu = \mu_0 + \eta\epsilon^2$ (see Eq. (2.7)). That is, the solution to Eq. (3.11) is $U = U(x, \kappa; \epsilon)$. An equivalent difficulty is that terms in the perturbation series solution (2.9) become harder to obtain at higher powers of ϵ . To overcome this difficulty, we approximate μ in (3.11) by its leading-order term μ_0 and get a further reduced integral equation

$$U_{xx} + 2i\kappa U_x + [\mu_0 - \kappa^2 - V(x)]U + 4\sigma \int_0^\kappa d\lambda U(x, \kappa - \lambda) \times \int_0^\lambda d\rho U(x, \lambda - \rho)U(x, \rho) = 0. \quad (3.12)$$

This integral equation does not depend on ϵ , thus its solution is a function of x and κ only, i.e., $U = U(x, \kappa)$. Notice that this $U(x, \kappa)$ solution to (3.12) is equal to the $U(x, \kappa; \epsilon)$ solution to (3.11) with ϵ set to zero, i.e., $U(x, \kappa) = U(x, \kappa; 0)$. The difference between solutions $U(x, \kappa)$ and $U(x, \kappa; \epsilon)$ of (3.11) and (3.12) is $O(\epsilon^2)$, which is subdominant and can be neglected.

The solution to the reduced integral equation (3.12) is now expanded into a power series in κ ,

$$U(x, \kappa) = \frac{a\beta}{2} \sum_{n=0}^{\infty} U_n(x) \kappa^n, \quad (3.13)$$

with

$$U_0 = p(x), \quad U_1 = iv(x), \dots, \quad (3.14)$$

in view of (3.6). Substituting Eq. (3.13) into (3.12), we obtain the following recurrence equation for $U_n(x)$,

$$\begin{aligned} & \frac{d^2 U_{n+2}}{dx^2} + [\mu_0 - V(x)]U_{n+2} \\ &= U_n - 2i \frac{dU_{n+1}}{dx} - \sigma a^2 \beta^2 \sum_{m=0}^n U_{n-m} \frac{(n-m)!}{(n+2)!} \\ & \times \sum_{r=0}^m U_{m-r} U_r (m-r)! r!, \end{aligned} \quad (3.15)$$

where $n = 0, 1, 2, \dots$. The asymptotic behavior of functions $U_n(x)$ for $n \gg 1$ plays an important role in our analysis. This behavior is not easy to obtain directly from the above recurrence relation, but it can be deduced alternatively from local analysis near singularities of $U(x, \kappa)$ (see below).

We should point out that the reduced integral equation (3.12) and its solution (3.13) are not valid near singularities of $U(x, \kappa)$. The correct behavior there should be derived separately from the original integral equation (3.9) (see the next subsection). On the other hand, the solution (3.13) to the reduced integral equation (3.12) must smoothly merge with the solution of the exact integral equation (3.9) in the vicinity of each singularity. This matching will yield the asymptotic behavior of the recurrence relation (3.15) for $n \gg 1$, and thereby the residues of the pole singularities of $U(x, \kappa)$ will be determined.

3.2. Behavior near singularities

Now we examine the singularities in the solution $U(x, \kappa; \epsilon)$ to the exact integral equation (3.9). This solution depends on ϵ as well as on (x, κ) , but we shall denote it as $U(x, \kappa)$ for simplicity.

First, we determine the locations of these singularities. Singularities are expected to occur near values of $\kappa = \kappa_0$ where the linear part of Eq. (3.9) is zero, i.e.,

$$U_{xx}^{(0)} + 2i\kappa_0 U_x^{(0)} + [\mu_0 - \kappa_0^2 - V(x)]U^{(0)} = 0. \quad (3.16)$$

Writing $U^{(0)}(x) = e^{-i\kappa_0 x} \tilde{U}^{(0)}(x)$, we find that $\tilde{U}^{(0)}(x)$ satisfies the equation

$$\tilde{U}_{xx}^{(0)} + [\mu_0 - V(x)]\tilde{U}^{(0)} = 0, \quad (3.17)$$

whose solution is $\tilde{U}^{(0)}(x) = p(x)$, hence $U^{(0)}(x) = e^{-i\kappa_0 x} p(x)$. Since the spatial period of the solution $U^{(0)}(x)$ should match that of the solution (3.6), $U^{(0)}(x)$ and $p(x)$ should have the same periodicity. The period of $p(x)$ is either π or 2π , depending on whether the band edge is located at $k = 0$ or $k = \pm 1$ in the Brillouin zone. When $p(x)$ is π -periodic, it follows from (2.5) that $p(x) = \tilde{p}(x; \mu_0)$. Therefore, in order for $U^{(0)}(x) = e^{-i\kappa_0 x} \tilde{p}(x; \mu_0)$ to be π -periodic, $\kappa_0 = \pm 2$. When $p(x)$ is 2π -periodic, $p(x) = e^{\pm ix} \tilde{p}(x; \mu_0)$. Then, in order for $U^{(0)}(x) = e^{-i(\kappa_0 \mp 1)x} \tilde{p}(x; \mu_0)$ to be 2π -periodic, $\kappa_0 = \pm 2$ as well. Note that the solution $U(x, \kappa)$ can also have singularities near higher even integers $\kappa_0 = \pm 4, \pm 6, \dots$, but those singularities are weaker and are thus unnecessary to pursue. In the following, to avoid ambiguity, we set

$$\kappa_0 = 2. \quad (3.18)$$

Then the dominant singularities of the solution $U(x, \kappa)$ occur near $\kappa = \pm \kappa_0$.

Next, we determine the behavior of the solution $U(x, \kappa)$ near these singularities. For this purpose, we introduce the ‘‘inner’’ wave number

$$\xi = \frac{\kappa - \kappa_0}{\epsilon}, \quad (3.19)$$

that is, $\kappa = \kappa_0 + \epsilon \xi$. We also expand the solution $U(x, \kappa)$ near $\kappa = \kappa_0$ as

$$\begin{aligned} U(x, \xi) &= \frac{e^{-i\kappa_0 x}}{\epsilon^4} \{ \Phi_0(\xi) p(x) + i\epsilon \Phi_1(\xi) v(x) \\ &+ \epsilon^2 \Phi_2(\xi) f(x) + \dots \}, \end{aligned} \quad (3.20)$$

where $\xi = O(1)$. Here the fact that $U = O(\epsilon^{-4})$ is dictated by the $O(1/\xi^4)$ decay of function $\Phi_0(\xi)$ at large ξ (see Eq. (A.11) in Appendix A).

When $\kappa \sim \kappa_0$, the dominant contribution to the double integral in Eq. (3.9) comes from the region $\lambda \sim 0, \rho \sim 0$, and the regions $\lambda \sim \kappa, \rho \sim 0$ or $\rho \sim \kappa$. This dominant contribution can be calculated by using the leading-order term of the solution (3.20) near the singularity $\kappa \sim \kappa_0$ as well as the leading-order term of the solution (3.13) near $\kappa = 0$. Specifically, in the region of $\lambda \sim 0, \rho \sim 0$,

$$\begin{aligned} \cosh \frac{\pi \beta \kappa}{2\epsilon} &\approx \frac{1}{2} e^{\pi \beta \kappa / 2\epsilon}, \quad \cosh \frac{\pi \beta (\kappa - \lambda)}{2\epsilon} \approx \frac{1}{2} e^{\pi \beta (\kappa - \lambda) / 2\epsilon}, \\ U(x, \lambda - \rho) U(x, \rho) &\approx \frac{1}{4} a^2 \beta^2 p^2(x). \end{aligned} \quad (3.21)$$

Then, using scaled variables $\omega = \lambda/\epsilon, y = \rho/\epsilon$, the leading-order term of Eq. (3.20) as well as the formula

$$\int_{-\infty}^{\infty} \text{sech}(\omega - y) \text{sech} y dy = 2\omega \text{csch} \omega, \quad (3.22)$$

the contribution to the double integral in Eq. (3.9) from this region is

$$\frac{\sigma a^2 \beta^2}{2\epsilon^2} e^{-i\kappa_0 x} p^3(x) \int_{-\infty}^{\infty} \omega e^{\pi \beta \omega / 2} \text{csch} \frac{\pi \beta \omega}{2} \Phi_0(\xi - \omega) d\omega. \quad (3.23)$$

Turning next to the region $\lambda \sim \kappa$ and $\rho \sim 0$, through variable transformations $\hat{\lambda} = \kappa - \lambda, \hat{\rho} = \rho + \hat{\lambda}$ and exchange of order of integration, we find that the contribution to the double integral from this region is identical to (3.23). Likewise, the contribution from the region of $\lambda \sim \kappa$ and $\rho \sim \kappa$ is identical to (3.23) as well. Thus, under the change of variables

$$U(x, \kappa) = e^{-i\kappa_0 x} \tilde{U}(x, \kappa), \quad (3.24)$$

Eq. (3.9) then reduces to

$$\begin{aligned} \tilde{U}_{xx} + [\mu - V(x)]\tilde{U} + 2i\epsilon \xi \tilde{U}_x - \epsilon^2 \xi^2 \tilde{U} \\ + \frac{3}{2\epsilon^2} \sigma a^2 \beta^2 p^3(x) \int_{-\infty}^{\infty} \omega e^{\pi \beta \omega / 2} \text{csch} \frac{\pi \beta \omega}{2} \\ \times \Phi_0(\xi - \omega) d\omega = 0. \end{aligned} \quad (3.25)$$

Substituting the proposed local behavior (3.20) into (3.25), we find that the terms of order ϵ^{-4} are automatically balanced. At order ϵ^{-3} , we get

$$\Phi_1(\xi) \{ v_{xx} + [\mu_0 - V(x)]v \} = -2\xi \Phi_0(\xi) p_x, \quad (3.26)$$

hence, in view of (2.10),

$$\Phi_1(\xi) = \xi \Phi_0(\xi). \quad (3.27)$$

At order ϵ^{-2} , the linear inhomogeneous equation for $f(x)$ must satisfy a solvability condition, namely the forcing term must be orthogonal to the homogeneous solution $p(x)$. Utilizing the relation [5,10]

$$\int_0^{2\pi} [p(x) + 2v'(x)]p(x) dx = D \int_0^{2\pi} p^2(x) dx \quad (3.28)$$

as well as the expressions of μ and α in Eqs. (2.7) and (2.12), this solvability condition leads to the following integral equation for $\Phi_0(\xi)$,

$$\begin{aligned} (1 + \beta^2 \xi^2) \Phi_0(\xi) - 3\beta^2 \\ \times \int_{-\infty}^{\infty} \omega e^{\pi \beta \omega / 2} \text{csch} \frac{\pi \beta \omega}{2} \Phi_0(\xi - \omega) d\omega = 0. \end{aligned} \quad (3.29)$$

Under variable scalings

$$\tilde{\xi} = \beta \xi, \quad \tilde{\omega} = \beta \omega, \quad \tilde{\Phi}_0 = \Phi_0 / \beta^4, \quad (3.30)$$

this integral equation then becomes

$$(1 + \tilde{\xi}^2)\tilde{\Phi}_0(\tilde{\xi}) - 3 \int_{-\infty}^{\infty} \tilde{\omega} e^{\pi\tilde{\omega}/2} \operatorname{csch} \frac{\pi\tilde{\omega}}{2} \tilde{\Phi}_0(\tilde{\xi} - \tilde{\omega}) d\tilde{\omega} = 0. \quad (3.31)$$

Since the coefficient of $\tilde{\Phi}_0(\tilde{\xi})$ in Eq. (3.31) vanishes when $\tilde{\xi} = \pm i$, $\tilde{\Phi}_0(\tilde{\xi})$ is expected to have singularities at these two values of $\tilde{\xi}$.

Now we need to solve the integral equation (3.31). Coincidentally, this equation is equivalent to the integral equation appearing in the exponential asymptotics analysis of wave-packet solutions in the fifth-order KdV equation (see Eq. (5.3) in Ref. [34]). A solution to Eq. (3.31), which turns out to be correct, was obtained in [34] through formal calculations. However, a subtle issue that was not clarified in [34] is whether this formal solution in fact solves Eq. (3.31) everywhere in the complex $\tilde{\xi}$ -plane. In Appendix A, we will rigorously solve the integral equation (3.31), and show that its solution is

$$\tilde{\Phi}_0(\tilde{\xi}) = \frac{6}{1 + \tilde{\xi}^2} \int_{\mathcal{L}^\pm} \frac{1}{\sin^2 s} \phi(s) e^{-s\tilde{\xi}} ds, \quad (3.32)$$

with

$$\phi(s) = C \left(\frac{2}{\sin s} + \frac{\cos^2 s}{\sin s} - \frac{3s \cos s}{\sin^2 s} \right), \quad (3.33)$$

where the contours \mathcal{L}^\pm extend from 0 to $\pm i\infty$ for $\operatorname{Im}(\tilde{\xi}) < 0$ and $\operatorname{Im}(\tilde{\xi}) > 0$ respectively, and C is a constant. More importantly, we will show that even though this function $\tilde{\Phi}_0(\tilde{\xi})$ is analytic everywhere in the complex plane \mathbb{C} save for the two points $\tilde{\xi} = \pm i$ (where it has simple-pole singularities), it satisfies the integral equation (3.31) only outside the strip $-1 < \operatorname{Im}(\tilde{\xi}) < 1$ in the complex $\tilde{\xi}$ -plane.

The fact that the meromorphic function $\tilde{\Phi}_0(\tilde{\xi})$ satisfies the integral equation (3.31) outside the strip $|\operatorname{Im}(\tilde{\xi})| < 1$ but not inside it has important consequences: when we take the inverse Fourier transform to recover the physical solution $\psi(x, X)$, the path of integration should be chosen outside this strip. As we will see below, when the path of integration is chosen below this strip, the inverse Fourier transform will give a physical solution $\psi(x, X)$ which decays upstream but grows downstream due to the contribution from the pole at $\tilde{\xi} = -i$; this growing tail is precisely what we are seeking. If, on the other hand, the path of integration is chosen above this strip, the inverse Fourier transform will give a physical solution $\psi(x, X)$ which decays downstream but grows upstream. This is also a valid physical solution to the wave Eq. (2.3), but it is not the one consistent with the asymptotic behavior (3.1) and (3.2) we prescribed earlier. However, if the path of integration is chosen inside this strip, the inverse Fourier transform would give a localized function $\psi(x, X)$ which decays both upstream and downstream. This localized function matches the perturbation series solution (2.6) we constructed in Section 2, but it cannot be a true solution to the wave Eq. (2.3) precisely because the integral equation (3.31) does not have a solution inside the strip $|\operatorname{Im}(\tilde{\xi})| < 1$.

Another related point we would like to make is the following. As mentioned at the beginning of this section (below Eq. (3.3)), in anticipation of a growing tail of the form (3.2) in the solution $\psi(x, X)$, the Fourier transform (3.3) should be taken for complex wavenumbers K where $\operatorname{Im}(K) = -1/\beta$. Recalling that $\kappa = \epsilon K$ and the variable scalings (3.19) and (3.30), this Fourier transform then should be taken along the line $\operatorname{Im}(\tilde{\xi}) = -1$, which is the lower boundary of the strip $|\operatorname{Im}(\tilde{\xi})| < 1$. From the above analysis, we indeed have obtained the Fourier transform solution $\tilde{\Phi}_0(\tilde{\xi})$ along $\operatorname{Im}(\tilde{\xi}) = -1$, and the physical solution can be found by taking the inverse Fourier transform along this line. However, since the

solution $\tilde{\Phi}_0(\tilde{\xi})$ is analytic everywhere below the line $\operatorname{Im}(\tilde{\xi}) = -1$, the inverse Fourier transform can be taken along any line below $\operatorname{Im}(\tilde{\xi}) = -1$.

Now we are ready to determine the local behavior of the Fourier transform $\hat{\psi}(x, K)$ near its singularities. Notice that the solution $\tilde{\Phi}_0(\tilde{\xi})$ has simple-pole singularities at $\tilde{\xi} = \pm i$. Specifically, at both points, the integral in (3.32) is equal to $-C/6$; hence

$$\tilde{\Phi}_0(\tilde{\xi}) \rightarrow -\frac{C}{1 + \tilde{\xi}^2} \quad (\tilde{\xi} \rightarrow \pm i). \quad (3.34)$$

Then, from Eq. (3.34) as well as the variable scalings (3.30), we see that

$$\Phi_0(\xi) \rightarrow -\frac{C\beta^4}{1 + \beta^2\xi^2} \quad \left(\xi \rightarrow \mp \frac{i}{\beta} \right). \quad (3.35)$$

Therefore $\Phi_0(\xi)$ has simple poles at $\xi = \pm i/\beta$, and

$$\Phi_0(\xi) \rightarrow \mp \frac{1}{2} i \frac{\beta^3 C}{\xi \pm i/\beta} \quad \left(\xi \rightarrow \mp \frac{i}{\beta} \right). \quad (3.36)$$

Recalling Eqs. (3.19) and (3.20), we get

$$U \sim \mp i \frac{1}{2} \frac{\beta^3 C}{\epsilon^4} \frac{e^{-i\kappa_0 x}}{K - \frac{\kappa_0}{\epsilon} \pm \frac{i}{\beta}} p(x) \quad \left(K \rightarrow \frac{\kappa_0}{\epsilon} \mp \frac{i}{\beta} \right). \quad (3.37)$$

Finally, from Eq. (3.5), we obtain the local behavior of $\hat{\psi}(x, K)$ near $K = \kappa_0/\epsilon \mp i/\beta$:

$$\hat{\psi} \sim \frac{\beta^3 C}{\epsilon^3} e^{-\pi\beta\kappa_0/2\epsilon} e^{\mp X_0/\beta} \frac{e^{-i\kappa_0(x+X_0)}}{K - \frac{\kappa_0}{\epsilon} \pm \frac{i}{\beta}} p(x) \quad \left(K \rightarrow \frac{\kappa_0}{\epsilon} \mp \frac{i}{\beta} \right). \quad (3.38)$$

Moreover, from the symmetry of the Fourier transform $\hat{\psi}(x, K) = \hat{\psi}^*(x, -K^*)$ for real functions $\psi(x, X)$, it follows that

$$\hat{\psi} \sim -\frac{\beta^3 C^*}{\epsilon^3} e^{-\pi\beta\kappa_0/2\epsilon} e^{\mp X_0/\beta} \frac{e^{i\kappa_0(x+X_0)}}{K + \frac{\kappa_0}{\epsilon} \pm \frac{i}{\beta}} p(x) \quad \left(K \rightarrow -\frac{\kappa_0}{\epsilon} \mp \frac{i}{\beta} \right). \quad (3.39)$$

3.3. Inversion of Fourier transform

Lastly, we take the inverse Fourier transform of $\hat{\psi}(x, K)$ to obtain the physical solution $\psi(x, X)$:

$$\psi(x, X) = \int_{\mathcal{C}} \hat{\psi}(x, K) e^{iKX} dK, \quad (3.40)$$

where the contour \mathcal{C} is the line $\operatorname{Im}(K) = -1/\beta$. In view of the comments above, this contour should pass below the poles at $K = \pm\kappa_0/\epsilon - i/\beta$. It should also pass above the pole singularity $K = -i/\beta$ of the $\operatorname{sech}(\pi\beta K/2)$ term in Eq. (3.5) so that the physical solution $\psi(x, X)$ has the desired upstream behavior in (3.1). Then when $X \ll -1$ (upstream), by completing the contour \mathcal{C} with a large semicircle in the lower half plane, the dominant contribution to the inverse Fourier transform (3.40) comes from the pole at $K = -i/\beta$, and the wave profile far upstream is found to be exactly the same as that prescribed in Eq. (3.1). On the other hand, when $X \gg 1$ (downstream), by completing the contour \mathcal{C} with a large semicircle in the upper half plane, we pick up contributions from pole singularities at $K = \pm\kappa_0/\epsilon - i/\beta$, as well as the contribution from the pole singularity of $\operatorname{sech}(\pi\beta K/2)$ at $K = i/\beta$. In this process, we get contributions from other poles such as

$K = \pm\kappa_0/\epsilon + i/\beta$ as well, but those contributions are subdominant and can be neglected. Collecting the pole contributions from $K = \pm\kappa_0/\epsilon - i/\beta$ and $K = i/\beta$ and recalling $\kappa_0 = 2$, the wave profile of the solution far downstream is then found to be

$$\psi \sim 2\epsilon a e^{-(x-x_0)/\beta} p(x) + \frac{4\pi\beta^3\widehat{C}}{\epsilon^3} e^{-\pi\beta/\epsilon} \sin(2x_0 - \theta) e^{(x-x_0)/\beta} p(x), \quad x \gg 1/\epsilon. \quad (3.41)$$

Here, $\widehat{C} > 0$ and θ are the amplitude and phase of the constant C (which is complex in general), i.e.,

$$C = \widehat{C} e^{i\theta}. \quad (3.42)$$

The above formula (3.41) is one of the key results in this paper. It shows that the solution to Eq. (2.3) which decays upstream in general comprises a growing tail downstream. The amplitude of this growing tail is exponentially small in ϵ , and thus is not captured by the perturbation series expansion (2.6). However, this growing tail will vanish when

$$\sin(2x_0 - \theta) = 0. \quad (3.43)$$

In this case, the solution $\psi(x)$ becomes a truly localized gap soliton. Eq. (3.43) will be satisfied if and only if

$$x_0 = \theta/2, \quad (\theta + \pi)/2. \quad (3.44)$$

Since the lattice is π -periodic, all other values of x_0 which differ from those in (3.44) by multiples of π do not correspond to new gap soliton solutions. Therefore, precisely two gap solitons can bifurcate out from a Bloch-band edge, and the centers of their envelopes are given by Eq. (3.44). These two gap solitons are the counterparts of on-site and off-site gap solitons for a symmetric potential reported in the literature [7–11].

3.4. Calculation of the constant C

It remains to explain how to calculate the constant C , whose phase θ gives the soliton's locations in Eq. (3.44) and whose amplitude \widehat{C} gives the growing-tail amplitude in Eq. (3.41). As noted earlier, C cannot be determined from local analysis around the singularities $\kappa \sim \kappa_0$ alone, but has to be obtained by matching the local behavior of $U(x, \kappa)$ near the singularities with the power-series solution (3.13) away from the singularities. Specifically, the limit of the inner solution (3.20) as $\xi \rightarrow \infty$ must match the outer solution (3.13). Combining expansion (3.20) with the asymptotic behavior of $\widetilde{\Phi}_0(\xi)$ as $\xi \rightarrow \infty$ (see (A.11) in Appendix A) and recalling the various variable scalings, we find that

$$U(x, \kappa) \sim \frac{12C}{5} \frac{p(x)}{(\kappa - \kappa_0)^4} e^{-i\kappa_0 x}, \quad \kappa \sim \kappa_0, \quad (3.45)$$

or

$$U \sim \frac{12\widehat{C}}{5} \frac{p(x)}{(\kappa - \kappa_0)^4} [\cos(\kappa_0 x - \theta) - i \sin(\kappa_0 x - \theta)], \quad \kappa \sim \kappa_0 \quad (3.46)$$

in view of the expression of C in (3.42). In addition, due to the symmetry relation $U(x, \kappa) = U^*(x, -\kappa^*)$ for real functions $\psi(x, X)$, we get

$$U \sim \frac{12\widehat{C}}{5} \frac{p(x)}{(\kappa + \kappa_0)^4} [\cos(\kappa_0 x - \theta) + i \sin(\kappa_0 x - \theta)], \quad \kappa \sim -\kappa_0. \quad (3.47)$$

These behaviors should match the outer solution (3.13). From the expressions for U_0 and U_1 in Eq. (3.14) as well as the recurrence relation (3.15), it is clear that all even terms, U_{2m} , are purely real, and all odd terms, U_{2m+1} , are purely imaginary. Accordingly, when

the solution $U(x, \kappa)$ near the singularities $\kappa = \pm\kappa_0$ is expanded into power series of κ , in order for all even terms in this expansion to be real and all odd terms to be purely imaginary, the dominant singular term in (3.46) and (3.47) should be of the form

$$U \sim \frac{192\kappa_0^4\widehat{C}}{5(\kappa^2 - \kappa_0^2)^4} \times \left[\cos(\kappa_0 x - \theta) - i \frac{\kappa}{\kappa_0} \sin(\kappa_0 x - \theta) \right] p(x), \quad \kappa \sim \pm\kappa_0. \quad (3.48)$$

This revised singular behavior agrees with (3.46) and (3.47) near the singularities, and it also gives the desired property when expanded into power series of κ . To match (3.48) with the asymptotic series (3.13), we first expand

$$\frac{1}{(\kappa^2 - \kappa_0^2)^4} = \frac{1}{3! \kappa_0^8} \sum_{m=0}^{\infty} \frac{(m+3)!}{m!} \frac{\kappa^{2m}}{\kappa_0^{2m}}. \quad (3.49)$$

Inserting this expansion into (3.48) and recognizing that the resulting power series from this dominant singular term should be consistent with the power series (3.13) as $n \rightarrow \infty$, the asymptotic behavior of U_n for $n \rightarrow \infty$ turns out to be

$$U_{2m} \sim \mathbb{D} \frac{m^3}{\kappa_0^{2m}} \cos(\kappa_0 x - \theta) p(x), \quad m \rightarrow \infty, \quad (3.50a)$$

$$U_{2m+1} \sim -i \mathbb{D} \frac{m^3}{\kappa_0^{2m+1}} \sin(\kappa_0 x - \theta) p(x), \quad m \rightarrow \infty, \quad (3.50b)$$

where

$$\widehat{C} = \frac{5}{4} a \beta \mathbb{D}. \quad (3.51)$$

Here the asymptotic behavior of $(m+3)!/m! \sim m^3$ for $m \gg 1$ has been used. Since $\widehat{C} > 0$, $\mathbb{D} > 0$ as well. The constants \mathbb{D} and θ in Eq. (3.50) can be determined by solving the recurrence equation (3.15) as discussed in Appendix B; the soliton's positions x_0 in (3.44) as well as the growing tail in (3.41) are thus completely specified.

It is noted that the above procedure for deriving the asymptotics (3.50) of the recurrence relation (3.15) differs from that followed in the study of solitary wave packets of the fifth-order KdV equation [34]. In the earlier approach, this asymptotics would be derived by matching the power-series solution (3.13) with the local behavior near singularities of the *approximate* integral equation (3.12). Accordingly, the singularities of the approximate integral equation (3.12) would need to be studied as well. In the present treatment, the asymptotics (3.50) was derived by matching the power-series solution (3.13) directly with the local behavior near the singularities of the *exact* integral equation (3.9). As a result, the singularity analysis of the approximate integral equation (3.12) is no longer necessary, and the exponential asymptotics technique in the wavenumber domain is somewhat simplified and streamlined.

For symmetric periodic potentials $V(x)$, the constant θ can be obtained without solving the recurrence relation (3.15). In this case, as remarked earlier, the Bloch wave $p(x)$ is always either symmetric or anti-symmetric in x , and $v(x)$ has the opposite parity of $p(x)$. Then, from the recurrence relation (3.15), it is easy to check that U_{2m} would always have the same parity as $p(x)$, and U_{2m+1} would always have the opposite parity of $p(x)$. Therefore, C is real and $\theta = 0$ or π ; so from (3.44), the two gap solitons are located at $x_0 = 0, \quad \pi/2.$ (3.52)

This reproduces the result obtained in [10] for a $\sin^2 x$ potential (see also [6]).

4. Linear-stability eigenvalues

In this section, we examine the linear stability of the two families of gap solitons near band edges obtained in the previous section. The growing-tail formula (3.41) turns out to be useful in this stability analysis as well. The approach taken here parallels that followed in [35] for the stability of elevation and depression solitary wavepackets of the fifth-order KdV equation.

Let $\psi_s(x)$ be the gap soliton of Eq. (2.3) given by Eq. (2.9), whose envelope $A(X)$ is centered at $x_0 = x_{0s}$, where x_{0s} is one of the two positions given in Eq. (3.44). To study the linear stability of this gap soliton, we linearize Eq. (2.1) around this basic state, and introduce perturbations in the form of normal modes:

$$U(x, t) = e^{-i\mu t} \{ \psi_s(x) + [v(x) - w(x)]e^{\lambda t} + [v^*(x) - w^*(x)]e^{\lambda^* t} \}, \quad (4.1)$$

where $v, w \ll 1$. Substituting this perturbed solution into Eq. (2.1) and neglecting higher order terms of (v, w) , we obtain the linear-stability eigenvalue problem

$$L_0 w = -i\lambda v, \quad L_1 v = -i\lambda w, \quad (4.2)$$

where

$$L_0 = \frac{d^2}{dx^2} - V(x) + \mu + \sigma \psi_s^2, \quad (4.3)$$

and

$$L_1 = \frac{d^2}{dx^2} - V(x) + \mu + 3\sigma \psi_s^2. \quad (4.4)$$

If there exist eigenvalues λ with positive real parts, then this gap solution is linearly unstable. Otherwise, it is linearly stable.

Near a band edge, the gap soliton given by Eq. (2.9) is a low-amplitude Bloch-wave packet whose envelope is governed by Eq. (2.11). As this envelope equation is translation invariant, the linearization spectrum of its soliton solution (2.14) contains a zero eigenvalue induced by this translation invariance. In the full lattice Eq. (2.1), however, the translation invariance is destroyed, and thus this zero eigenvalue associated with spatial translations must bifurcate out. Our goal here is to calculate this eigenvalue bifurcation when the gap soliton bifurcates out from the Bloch-band edge. It will turn out that this bifurcation occurs along the imaginary and real axes respectively for the two gap solitons in (3.44). As a result, the gap soliton at $x_0 = \theta/2$ is linearly stable, while the one at $x_0 = (\theta + \pi)/2$ is linearly unstable. Moreover, asymptotically accurate formulae for these eigenvalues will be derived, confirming that these eigenvalues are exponentially small in the soliton's amplitude ϵ .

We begin by eliminating w from the eigenvalue Eq. (4.2) and obtain the following single equation for v :

$$L_0 L_1 v = -\lambda^2 v. \quad (4.5)$$

Since the bifurcated eigenvalue λ is small near band edges, we expand the eigenfunction v into the following perturbation series

$$v = v_0 + \lambda^2 v_1 + \lambda^4 v_2 + \dots \quad (4.6)$$

Inserting this expansion into Eq. (4.5), at $O(1)$ we get

$$L_0 L_1 v_0 = 0. \quad (4.7)$$

To determine the solution v_0 , we recall from Eqs. (2.3) and (4.3) and the analysis of the previous section that

$$L_0 \psi(x; x_0) = 0, \quad (4.8)$$

where $\psi(x; x_0)$ is the nonlocal solution to Eq. (2.3) whose envelope function $A(X)$ is centered at $x = x_0$. Taking the derivative of Eq. (4.8) with respect to x_0 and then setting $x_0 = x_{0s}$, we obtain

$$L_1 \left. \frac{\partial \psi}{\partial x_0} \right|_{x_0=x_{0s}} = 0, \quad (4.9)$$

so the solution to Eq. (4.7) is

$$v_0 = \left. \frac{\partial \psi}{\partial x_0} \right|_{x_0=x_{0s}}. \quad (4.10)$$

Using the downstream asymptotics of the solution $\psi(x; x_0)$ in Eq. (3.41), we find that

$$v_0 \sim \frac{2\epsilon^2 a}{\beta} e^{-(x-x_{0s})/\beta} p(x) + \frac{8\pi\beta^3 \widehat{C}}{\epsilon^3} e^{-\pi\beta/\epsilon} \times \cos(2x_{0s} - \theta) e^{(x-x_{0s})/\beta} p(x), \quad x \gg 1/\epsilon, \quad (4.11)$$

where $X_{0s} = \epsilon x_{0s}$. Notice that this function v_0 has a growing tail downstream. Since our eigenfunction $v(x)$ must be a localized function, this growing tail in v_0 will be balanced later by the $\lambda^2 v_1$ term in (4.6), thereby providing the desired formula for the eigenvalue λ . Since the growing tail in v_0 is exponentially small, λ will thus be exponentially small as well.

Now we determine the solution v_1 . The equation for v_1 can be obtained from Eq. (4.5) at $O(\lambda^2)$ as

$$L_0 L_1 v_1 = -v_0, \quad (4.12)$$

or

$$L_1 v_1 = w_0, \quad (4.13)$$

and

$$L_0 w_0 = -v_0. \quad (4.14)$$

To determine w_0 from (4.14), we notice that the growing tail in v_0 is exponentially small, thus it will be neglected in this calculation of w_0 . The homogeneous equation of (4.14) has a localized solution $\psi_s(x, X)$. Notice that v_0 in (4.10) can be rewritten as $-\epsilon \partial \psi / \partial X|_{x_0=x_{0s}}$; thus the solvability condition of Eq. (4.14) is

$$\int_{-\infty}^{\infty} \left. \frac{\partial \psi^2(x, X)}{\partial X} \right|_{x_0=x_{0s}} dx = 0. \quad (4.15)$$

Here the integration is with respect to the original x variable, not the fast variable x . Inserting the perturbation series solution (2.9) into (4.15), we can see that all terms in this integral are of the form

$$\int_{-\infty}^{\infty} F'(X) q(x) dx, \quad (4.16)$$

where $F(X)$ is a localized function of the slow variable X , and $q(x)$ is a periodic function of x . Expanding $q(x)$ into a Fourier series, one can see that this integral is exponentially small in ϵ . Thus the solvability condition (4.15) is satisfied to all orders of ϵ , hence a localized solution can be found for w_0 (when exponentially small terms are neglected). To determine this localized solution, we notice from the expression (4.10) for v_0 and the perturbation series expansion (2.9) that the leading-order approximation for v_0 is

$$v_0 \sim -\epsilon^2 A'(X) p(x). \quad (4.17)$$

Here the function $A(X)$ is given in Eq. (2.14) with $X_0 = X_{0s}$. The solution w_0 to Eq. (4.14) can be expanded into a perturbation series

$$w_0 = B(X) p(x) + \epsilon B'(X) v(x) + \epsilon^2 \widehat{w}_0(x, X) + \dots \quad (4.18)$$

Inserting this expansion as well as the perturbation series solution (2.9) into Eq. (4.14), the terms of $O(1)$ and $O(\epsilon)$ are automatically

balanced. At $O(\epsilon^2)$, we obtain the following equation for \widehat{w}_0 ,

$$\begin{aligned} \widehat{w}_{0xx} - V(x)\widehat{w}_0 + \mu_0\widehat{w}_0 \\ = -[p(x) + 2v'(x)]B''(X) - \eta p(x)B(X) \\ - \sigma A^2(X)B(X)p^3(x) + A'(X)p(x). \end{aligned} \quad (4.19)$$

Imposing the solvability condition on this equation and utilizing the relation (3.28) as well as the expression of α in (2.12), we find that $B(X)$ satisfies the equation

$$D \frac{d^2 B}{dX^2} + \eta B + \sigma \alpha A^2 B = A'(X), \quad (4.20)$$

whose solution is

$$B(X) = \frac{1}{2D}(X - X_{0s})A(X). \quad (4.21)$$

Next, we determine the solution v_1 to Eq. (4.13). This equation has the homogeneous solution v_0 which is not orthogonal to the inhomogeneous term w_0 . Indeed, by approximating v_0 by its leading-order term (4.17) and w_0 by its leading-order term $B(X)p(x)$ in (4.18), we can easily see that the integral of $v_0 w_0$ from $x = -\infty$ to $+\infty$ is non-zero; hence the solvability condition of Eq. (4.13) is not met, indicating that the solution v_1 will be nonlocal. By requiring v_1 to be decaying upstream ($x \rightarrow -\infty$), then it will exhibit a growing tail downstream ($x \gg 1/\epsilon$). To determine this nonlocal solution, we introduce the perturbation series

$$v_1 = \frac{1}{\epsilon^2} \{F(X)p(x) + \epsilon F'(X)v(x) + \epsilon^2 \widehat{v}_1(x, X) + \dots\}. \quad (4.22)$$

Inserting this expansion as well as the perturbation series solution (2.9) into Eq. (4.13), the terms of $O(\epsilon^{-2})$ and $O(\epsilon^{-1})$ are automatically balanced. At $O(1)$, we obtain the following equation for \widehat{v}_1

$$\begin{aligned} \widehat{v}_{1xx} - V(x)\widehat{v}_1 + \mu_0\widehat{v}_1 \\ = -[p(x) + 2v'(x)]F''(X) - \eta p(x)F(X) \\ - 3\sigma A^2(X)F(X)p^3(x) + \frac{1}{2D}(X - X_{0s})A(X)p(x). \end{aligned} \quad (4.23)$$

Imposing the solvability condition on this equation and utilizing the relation (3.28) as well as the expression of α in (2.12), we find that $F(X)$ satisfies the equation

$$D \frac{d^2 F}{dX^2} + \eta F + 3\sigma \alpha A^2 F = \frac{1}{2D}(X - X_{0s})A. \quad (4.24)$$

By differentiating the envelope Eq. (2.11) with respect to X , we see that $A'(X)$ is a homogeneous solution of Eq. (4.24). This homogeneous solution is not orthogonal to the inhomogeneous term; hence, the forced problem (4.24) has no locally confined solution. By requiring $F(X) \rightarrow 0$ as $X \rightarrow -\infty$, then $F(X)$ will exponentially grow downstream as

$$F(X) \rightarrow R e^{(X-X_{0s})/\beta}, \quad X \gg 1, \quad (4.25)$$

where R is a constant. To determine R , we multiply Eq. (4.24) by its homogeneous solution $A'(X)$ and then integrate it from $-\infty$ to X :

$$\begin{aligned} \int_{-\infty}^X A'(\tilde{X})[DF''(\tilde{X}) + \eta F(\tilde{X}) + 3\sigma \alpha A^2(\tilde{X})F(\tilde{X})]d\tilde{X} \\ = \frac{1}{2D} \int_{-\infty}^X (\tilde{X} - X_{0s})A(\tilde{X})A'(\tilde{X})d\tilde{X}. \end{aligned} \quad (4.26)$$

Performing integration by parts to the left side of Eq. (4.26), taking $X \gg 1$ and using the asymptotics (4.25) as well as the expression (2.14) for $A(X)$, Eq. (4.26) then gives $R = a/8\beta$; therefore, (4.25) becomes

$$F(X) \rightarrow \frac{a}{8\beta} e^{(X-X_{0s})/\beta}, \quad X \gg 1. \quad (4.27)$$

Substituting this $F(X)$ into the expansion (4.22), we then obtain

$$v_1 \sim \frac{a}{8\beta} \frac{e^{(X-X_{0s})/\beta}}{\epsilon^2} p(x), \quad X \gg 1. \quad (4.28)$$

Inserting this growing tail and the growing tail of v_0 in (4.11) into the expansion (4.6) and requiring these two growing tails to balance each other, we then obtain the eigenvalue formula

$$\lambda^2 = -\frac{64\pi\beta^4\widehat{C}}{a} \cdot \frac{e^{-\pi\beta/\epsilon}}{\epsilon} \cos(2x_{0s} - \theta). \quad (4.29)$$

Replacing \widehat{C} by the formula (3.51), our final eigenvalue formula is then

$$\lambda^2 = -80\pi\mathbb{D}\beta^5 \cdot \frac{e^{-\pi\beta/\epsilon}}{\epsilon} \cos(2x_{0s} - \theta). \quad (4.30)$$

Here $\epsilon = \sqrt{|\mu - \mu_0|}$, constants \mathbb{D} and θ are computed from the recurrence relation (3.15) via the asymptotics (3.50), $\beta = \sqrt{|\mathbb{D}|}$, D is the second-order dispersion coefficient defined in (2.12), and x_{0s} is the location of gap solitons given in Eq. (3.44). For the two gap-soliton locations in (3.44), $\cos(2x_{0s} - \theta)$ is 1 and -1 respectively. Thus the gap soliton located at $x_{0s} = \theta/2$ is linearly stable, while the one located at $x_{0s} = (\theta + \pi)/2$ is linearly unstable. For the unstable gap soliton, the formula for the unstable eigenvalue is

$$\lambda_{\text{unstable}} = \sqrt{80\pi\mathbb{D}\beta^5} \cdot \frac{e^{-\pi\beta/2\epsilon}}{\sqrt{\epsilon}}, \quad (4.31)$$

which is purely real and exponentially small in the soliton amplitude ϵ . For the stable gap soliton, the eigenvalue is purely imaginary, and its magnitude is the same as that given in (4.31).

5. Numerical results

In this section, we present numerical results on gap solitons and their linear-stability eigenvalues, and make a comparison against the above analytical results. In our computations, we take the periodic potential to be

$$V(x) = V_0 \sin^2 x, \quad (5.1)$$

which is symmetric in x . This potential is common in physical situations such as nonlinear optics and Bose–Einstein condensates. We also take the potential depth to be $V_0 = 6$. The band-gap structure for this potential has been obtained in [5,16] (see also Fig. 2 (left panel) in this paper). The numerical algorithms for computations of gap solitons and their stability eigenvalues can be found in [6].

5.1. The case of self-focusing nonlinearity

When $\sigma = 1$ (self-focusing nonlinearity), gap solitons can bifurcate from the lower edge $\mu_0 = 2.0613182$ of the first Bloch band, where the dispersion coefficient $D = 0.4348$. In this case,

$$a = 1.7146, \quad \beta = \sqrt{D} = 0.6594. \quad (5.2)$$

To determine \mathbb{D} and θ , we solve the recurrence relation (3.15) numerically. The procedure of this numerical computation is described in Appendix B, and the result is shown in Fig. 1. This figure shows that U_{2m} and U_{2m+1} indeed approach the asymptotic states (3.50), with the parameters

$$\mathbb{D} = 0.925, \quad \theta = 0.$$

According to (3.44), the gap solitons are located at $x_{0s} = 0$ and $\pi/2$, consistent with our earlier result (3.52) since the potential (5.1) is symmetric. The gap solitons located at $x_{0s} = 0$ (potential minimum) are on-site solitons, and gap solitons located at $x_{0s} = \pi/2$

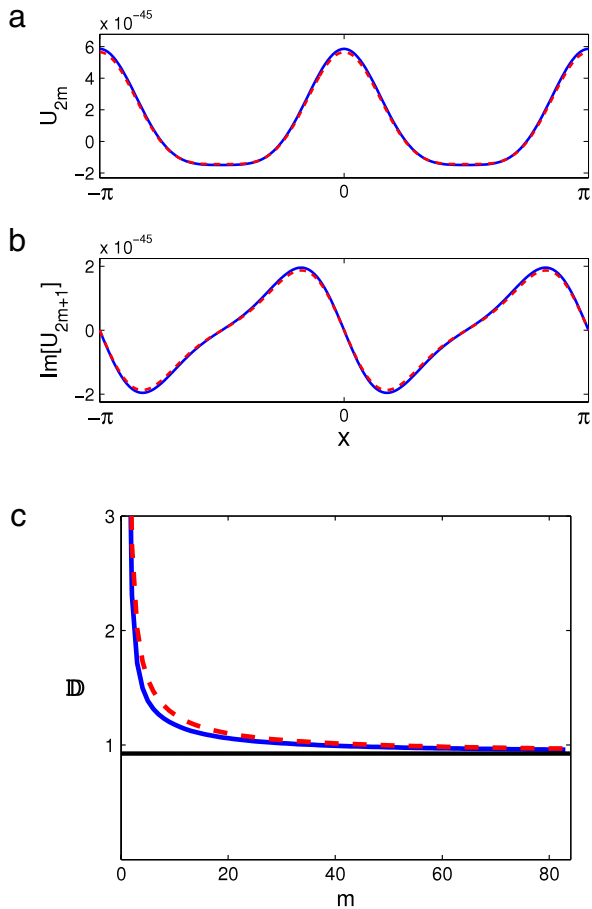


Fig. 1. Solutions of the recurrence relation (3.15) for $\sigma = 1$ and $V_0 = 6$. (a,b) Numerical solutions U_{2m} and $\text{Im}(U_{2m+1})$ at $m = 83$ (solid blue curves); (c) the ratio between the maxima of $U_{2m}(x)$ and $m^3 2^{-2m} \cos 2xp(x)$ (solid blue curve) and the ratio between the maxima of $\text{Im}(U_{2m+1})(x)$ and $m^3 2^{-(2m+1)} \sin 2xp(x)$ (dashed red curve) versus m . These ratios approach the asymptotic value $\mathbb{D} = 0.925$ (horizontal black line) at large m . The asymptotic solutions (3.50) at $m = 83$ are also plotted in (a,b) (dashed red curves) for comparison. (For interpretation of the references to colour in this figure legend, the reader is referred to the web version of this article.)

(potential maximum) are off-site solitons. Numerically, we have indeed found these two families of gap solitons, and their solution profiles and power curves are displayed in Fig. 2.

Since $\theta = 0$, according to our analysis, the on-site gap solitons are linearly stable, and off-site solitons are linearly unstable. Numerically we have computed the whole stability spectra for the on-site and off-site solitons at $\mu = 2$, and these spectra are displayed in Fig. 3(a) and (b). These spectra confirm that the on-site soliton is linearly stable, and the off-site soliton is linearly unstable due to a real positive eigenvalue. Now we compare this numerical unstable eigenvalue with our analytical formula (4.31) for various values of ϵ . Using the above parameter values, we find that the theoretical eigenvalue formula (4.31) for off-site solitons is

$$\lambda_{\text{anal}} = 5.38 \frac{e^{-\pi\beta/2\epsilon}}{\sqrt{\epsilon}}. \quad (5.3)$$

This theoretical formula is displayed in Fig. 3(d) (as solid line). The numerically obtained eigenvalue λ versus ϵ is also displayed in Fig. 3(d) (as dots). It is seen that the numerical eigenvalues approach this analytical formula when $\epsilon \rightarrow 0$. Closer examination of these numerical eigenvalues shows that,

$$\lambda_{\text{num}} \rightarrow 5.38 \frac{e^{-\pi\beta/2\epsilon}}{\sqrt{\epsilon}}, \quad \epsilon \rightarrow 0. \quad (5.4)$$

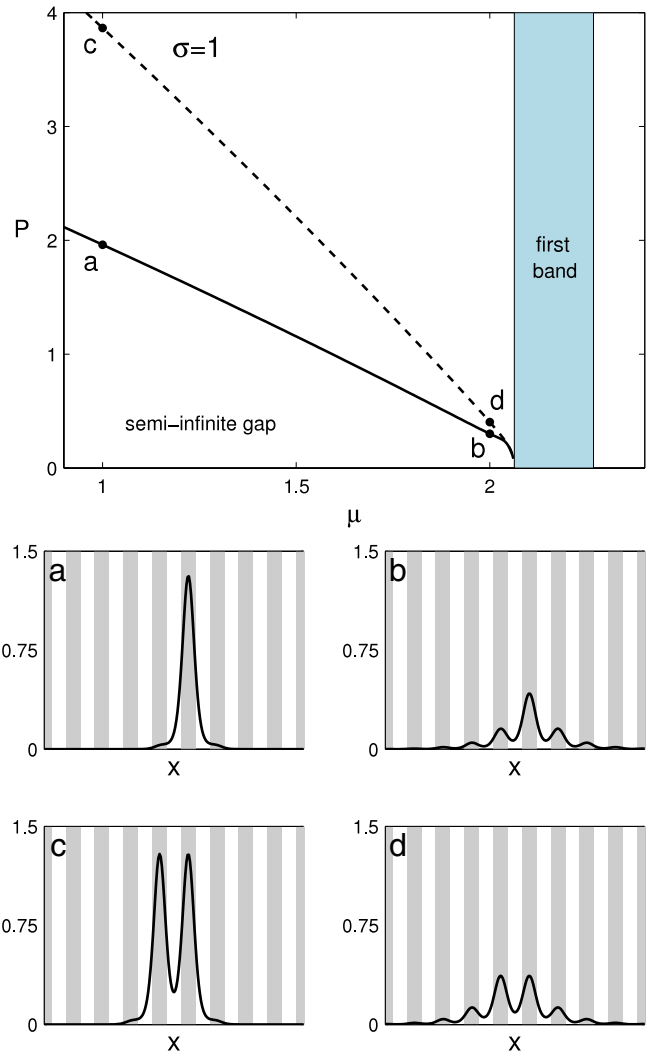


Fig. 2. On-site and off-site solitons bifurcated from the lower edge of the first Bloch band under self-focusing nonlinearity ($\sigma = 1$, $V_0 = 6$). Top panel: the power curves (solid curve: on-site solitons; dashed curve: off-site solitons); (a–d): profiles of solitons at points marked by the same letters on the power curves ($\mu = 1$ in (a, c) and $\mu = 2$ in (b, d)). The vertical gray stripes represent lattice sites (locations of low potentials).

Thus, the numerical eigenvalues and the analytical formula (5.3) for $\epsilon \ll 1$ are in excellent agreement, confirming that our analytical eigenvalue formula (4.31) is asymptotically accurate.

For on-site solitons, the eigenvalues $\pm\lambda$ from formula (4.30) are purely imaginary. One may wonder why these purely imaginary discrete eigenvalues are not present in the spectrum of Fig. 3(a) at $\mu = 2$. The reason can be seen in Fig. 3(c). What happens is that when μ just bifurcates off from μ_0 (i.e., when ϵ is very small), a pair of purely imaginary discrete eigenvalues $\pm\lambda$ indeed bifurcates out from zero. These eigenvalues are displayed in Fig. 3(c), where $i\lambda$ is plotted (to make it real). After bifurcation, these eigenvalues move along the imaginary axis toward the continuous-eigenvalue bands, and at $\epsilon \approx 0.2$, or $\mu \approx 2.02$, they merge into the continuous spectrum and disappear. For this reason, these eigenvalues are absent in the spectrum of Fig. 3(a) at $\mu = 2$. At small ϵ values where these stable eigenvalues still exist, we can compare the numerical results with our analytical formula (4.30). In this case, the analytical formula (4.30) gives

$$\lambda_{\text{anal}} = \pm 5.38i \frac{e^{-\pi\beta/2\epsilon}}{\sqrt{\epsilon}}, \quad \epsilon \ll 1. \quad (5.5)$$

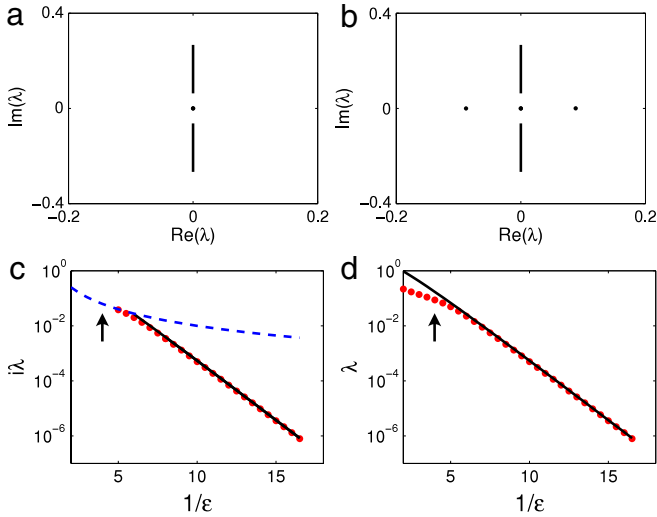


Fig. 3. (a, b) Spectra of the on-site and off-site gap solitons shown in Fig. 2(b, d) at $\mu = 2$ respectively; (c, d) comparison of analytical and numerical discrete eigenvalues for on-site and off-site solitons of Fig. 2 near the lower band edge $\mu_0 = 2.0613182$ under self-focusing nonlinearity ((c) for on-site solitons and (d) for off-site solitons). Here $\epsilon = \sqrt{\mu_0 - \mu}$. Dots: numerical values; solid lines: analytical formulae (5.5) in (c) and (5.3) in (d); the dashed line in (c) is the edge of the continuous spectrum on the imaginary axis. The corresponding $1/\epsilon$ value for the spectra in (a, b) is marked by arrows in (c, d).

This formula is shown in Fig. 3(c) by a solid line. The numerical eigenvalues are also shown in this figure as dots. Examination of the numerical eigenvalues shows that

$$\lambda_{\text{num}} \rightarrow \pm 5.381 \frac{e^{-\pi\beta/2\epsilon}}{\sqrt{\epsilon}}, \quad \epsilon \rightarrow 0, \quad (5.6)$$

again in excellent agreement with the analytical formula.

5.2. The case of self-defocusing nonlinearity

Next, we present numerical results for the case of self-defocusing nonlinearity ($\sigma = -1$), and compare them with the analytical results. In this case, gap solitons can bifurcate from the upper edge $\mu_0 = 2.266735$ of the first Bloch band. The dispersion coefficient at this edge is $D = -0.5881$, and

$$a = 1.681, \quad \beta = \sqrt{|D|} = 0.7669. \quad (5.7)$$

Solving the recurrence Eq. (3.15) numerically, we find that U_{2m} and U_{2m+1} approach the asymptotic states (3.50) with the parameters

$$\mathbb{D} = 1.870, \quad \theta = 0.$$

Thus the gap solitons are located at $x_{0s} = 0$ and $\pi/2$, as with self-focusing nonlinearity in the previous subsection. Numerically, we have found these two families of gap solitons, and their solution profiles and power curves are displayed in Fig. 4. Since $\theta = 0$, the on-site gap solitons are again linearly stable, and off-site solitons are linearly unstable according to our analysis. This is confirmed in Fig. 5(a) and (b), where the stability spectra for the on-site and off-site solitons at $\mu = 2.35$ are displayed. Now we make quantitative comparison between the numerical eigenvalues and the theoretical formula (4.30). For the off-site solitons, using the \mathbb{D} and β values given above, the theoretical formula (4.31) for the unstable eigenvalue λ becomes

$$\lambda_{\text{anal}} = 11.17 \frac{e^{-\pi\beta/2\epsilon}}{\sqrt{\epsilon}}, \quad \epsilon \ll 1. \quad (5.8)$$

This theoretical formula is displayed in Fig. 5(d) (solid line). The numerically obtained eigenvalue λ versus ϵ is also displayed in

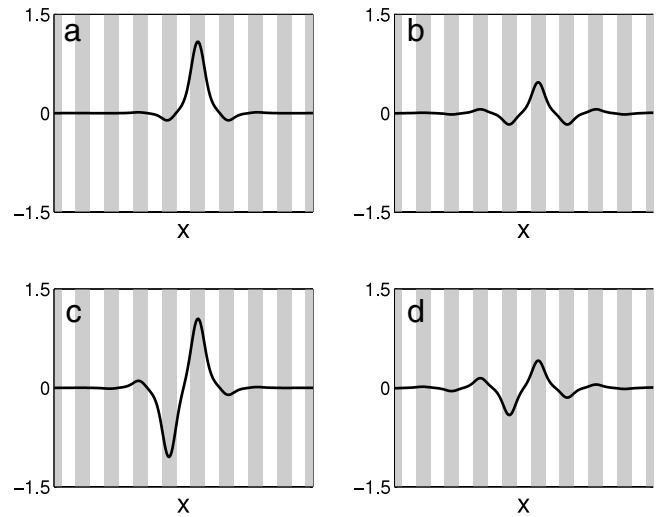
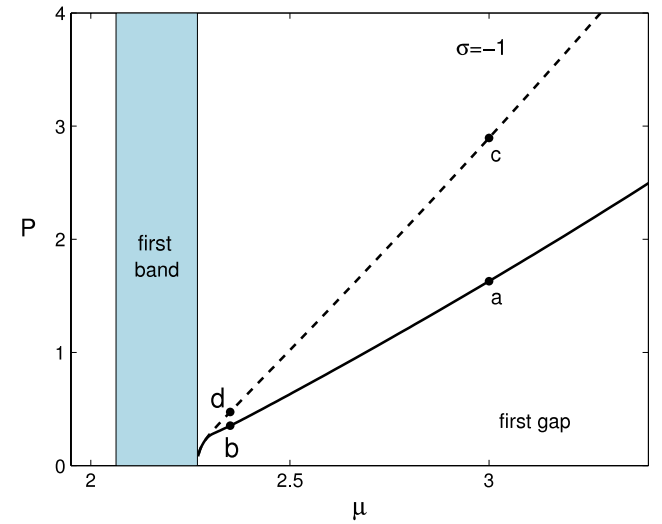


Fig. 4. On-site and off-site solitons bifurcated from the upper edge of the first Bloch band under self-defocusing nonlinearity ($\sigma = -1$, $V_0 = 6$). Top panel: the power curves (solid curve: on-site solitons; dashed curve: off-site solitons); (a–d): profiles of solitons at points marked by the same letters on the power curves ($\mu = 3$ in (a, c) and $\mu = 2.35$ in (b, d)). The vertical gray stripes represent lattice sites.

Fig. 5(d) (dots). For this defocusing case, the numerical eigenvalues also approach the analytical formula when $\epsilon \rightarrow 0$. Closer examination of these numerical eigenvalues shows that

$$\lambda_{\text{num}} \approx 11.18 \frac{e^{-\pi\beta/2\epsilon}}{\sqrt{\epsilon}}, \quad \epsilon \rightarrow 0, \quad (5.9)$$

which agrees with the analytical formula (5.8) very well. We have also compared the numerical imaginary eigenvalues and the analytical formula (4.30) for on-site solitons in Fig. 5(c). Here again, excellent agreement can be seen between them. These comparisons undoubtedly establish that the eigenvalue formula (4.30) for gap solitons is asymptotically accurate near band edges.

6. Summary and discussion

In this paper, we studied 1D gap solitons near band edges and their linear stability properties in general periodic potentials, using an exponential asymptotics method. We showed that in general π -periodic potentials, two gap solitons bifurcate from every Bloch-band edge, and these solitons are located at $x_0 = \theta/2$ and $(\theta + \pi)/2$, the parameter θ being determined from the asymptotics (3.50) of the recurrence relation (3.15). In the special

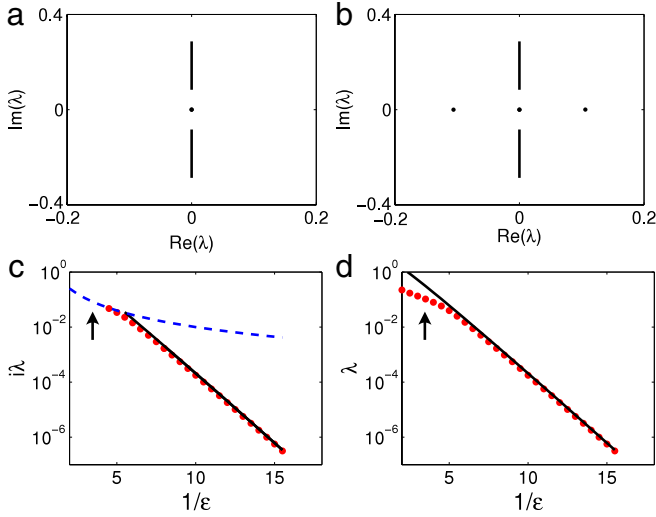


Fig. 5. (a, b) Spectra of the on-site and off-site gap solitons at $\mu = 2.35$ in Fig. 4(b, d) respectively; (c, d) comparison of analytical and numerical discrete eigenvalues for on-site and off-site solitons of Fig. 4 near the upper band edge $\mu_0 = 2.266735$ under self-defocusing nonlinearity ((c) for on-site solitons and (d) for off-site solitons). Here $\epsilon = \sqrt{\mu - \mu_0}$. Dots: numerical values; solid lines: analytical formulae (4.30) in (c) and (5.8) in (d); the dashed line in (c) is the edge of the continuous spectrum on the imaginary axis. The corresponding $1/\epsilon$ value for the spectra in (a,b) is marked by arrows in (c,d).

case when the potential is symmetric, we recover the well-known result that these solitons are located at $x_0 = 0$ and $\pi/2$, i.e., at the symmetry point and half a period away from it. We also studied the linear stability of gap solitons bifurcated from band edges and derived the asymptotically accurate eigenvalue formula (4.30). The coefficient \mathbb{D} in this formula is obtained from the asymptotics (3.50) of the recurrence relation (3.15). Our analysis shows that the eigenvalues are exponentially small in the soliton's amplitude, and out of the two gap soliton families that bifurcate out at a band edge, the one located at $x_0 = \theta/2$ is always linearly stable, while the other is always linearly unstable. Quantitative comparison between the eigenvalue formula and numerical results is also performed, and excellent agreement is observed. With the results obtained in this paper, thorough analytical understanding of gap solitons and their linear stability near band edges in general periodic potentials is now achieved. The present theory is based on an exponential asymptotics procedure in the wavenumber domain proposed in [34,35], and we have also clarified certain subtle issues in the original development of this technique, in addition to simplifying and streamlining the entire solution procedure.

In the analysis of this paper, the growing-tail formula (3.41) plays a critical role. This formula not only yields the positions of gap solitons, but also leads to the eigenvalue formula for the stability of gap solitons. The same formula proves useful for analytically constructing multi-Bloch-wave-packet gap solitons similar to the multi-packet solitary waves in the fifth-order KdV equation [34]. Such multi-Bloch-wave-packets do not bifurcate from band edges, thus their power curves exhibit multiple branches and do not touch band edges. As it is possible to combine individual Bloch-wave packets in an infinite number of ways, there is an infinity of multi-Bloch-wave-packet gap soliton families. Construction of such multi-Bloch-wave-packets in the stationary lattice Eq. (2.3) will be reported elsewhere [28].

Acknowledgements

The work of G.H. and J.Y. is supported in part by the Air Force Office of Scientific Research (Grant USAF 9550-09-1-0228) and the National Science Foundation (Grant DMS-0908167), and the work

of T.R.A. is supported in part by the National Science Foundation (Grant DMS-098122).

Appendix A. Solution to an integral equation

In this appendix, we rigorously solve the integral equation (3.31),

$$(1 + \xi^2)\tilde{\Phi}_0(\xi) - 3 \int_{-\infty}^{\infty} \tilde{\omega} e^{\pi\tilde{\omega}/2} \text{csch} \frac{\pi\tilde{\omega}}{2} \tilde{\Phi}_0(\xi - \tilde{\omega}) d\tilde{\omega} = 0. \quad (\text{A.1})$$

This equation is a linear homogenous equation. By moving the integral term to the right-hand side and then dividing both sides by $1 + \xi^2$, this equation can be viewed as an integral-operator eigenvalue equation with unit eigenvalue. To solve this equation, we notice that the integral in (A.1) is a convolution integral, which suggests posing the solution as

$$\tilde{\Phi}_0(\xi) = \int_{\mathcal{L}^{\pm}} e^{-s\xi} \phi(s) ds, \quad (\text{A.2})$$

where the contours \mathcal{L}^{\pm} extend from 0 to $\pm i\infty$ for $\text{Im}(\xi) < 0$ and $\text{Im}(\xi) > 0$, respectively. This is the same idea as was used in [34], except that here the paths of integration \mathcal{L}^{\pm} are explicitly specified so that the whole calculation becomes more concrete. This form of the solution is analogous to a Laplace transform, and the choice of different contours ensures that the exponential function $e^{-s\xi}$ decays at infinity so that the integral in (A.2) can converge.

Inserting the integral transform (A.2) into (A.1) and performing integration by parts, we get

$$\int_{\mathcal{L}^{\pm}} \left(\frac{d^2\phi}{ds^2} + \phi(s) \right) e^{-s\xi} ds - 3 \int_{-\infty}^{\infty} d\tilde{\omega} \times \int_{\mathcal{L}^{\pm}} ds \tilde{\omega} \text{csch} \frac{\pi\tilde{\omega}}{2} e^{\tilde{\omega}(s+\pi/2)} e^{-s\xi} \phi(s) = 0. \quad (\text{A.3})$$

In deriving the first integral in (A.3), we have assumed that $\phi(0) = \phi'(0) = 0$, which will be confirmed after the solution $\phi(s)$ has been obtained (see Eq. (A.8)). Now we wish to exchange the order of integration in the double integral in (A.3). Notice that its integrand is unbounded along the positive $\tilde{\omega}$ direction (for fixed s), hence this double integral is not absolutely convergent. In order to make this exchange of integration possible, we multiply this integrand by a function $e^{-\epsilon\tilde{\omega}}$, where $0 < \epsilon \ll 1$. The resulting integrand then becomes absolutely convergent, thus we can exchange its order of integration. After this exchange of integration, we utilize the formula

$$\int_{-\infty}^{\infty} \tilde{\omega} \text{csch} \frac{\pi\tilde{\omega}}{2} e^{\tilde{\omega}(s+\pi/2)-\epsilon\tilde{\omega}} d\tilde{\omega} = \frac{2}{\sin^2(s-\epsilon)}, \quad (\text{A.4})$$

and, in the end, we take the limit of $\epsilon \rightarrow 0^+$. After these manipulations, Eq. (A.3) becomes

$$\int_{\mathcal{L}^{\pm}} \left(\frac{d^2\phi}{ds^2} + \phi - \frac{6}{\sin^2 s} \phi \right) e^{-s\xi} ds = 0, \quad (\text{A.5})$$

whose solution $\phi(s)$ then solves the linear ordinary differential equation

$$\frac{d^2\phi}{ds^2} + \left(1 - \frac{6}{\sin^2 s} \right) \phi = 0. \quad (\text{A.6})$$

This linear ordinary differential equation has two linearly independent solutions [34]. One of them is $\phi(s) = \cos s / \sin^2 s$. This solution, however, is singular at $s = 0$, which makes the

integral in the transform (A.2) divergent, so it should be excluded. The other solution is

$$\phi(s) = C \left(\frac{2}{\sin s} + \frac{\cos^2 s}{\sin s} - \frac{3s \cos s}{\sin^2 s} \right), \quad (\text{A.7})$$

where C is a constant. This solution is non-singular at $s = 0$ since

$$\phi(s) \rightarrow \frac{2}{5}Cs^3, \quad s \rightarrow 0, \quad (\text{A.8})$$

and is our desired solution to Eq. (A.6). The asymptotics (A.8) also justifies our earlier derivation of the first integral in Eq. (A.3) by assuming $\phi(0) = \phi'(0) = 0$. It is important to notice that

$$\phi(s) \rightarrow \pm \frac{C}{21}e^{|s|}, \quad s \in \mathcal{L}^\pm \rightarrow \pm i\infty, \quad (\text{A.9})$$

implying that the integral transform in Eq. (A.2) is not convergent for $|\text{Im}(\xi)| \leq 1$. This means that the proposed solution $\tilde{\Phi}_0(\xi)$ given by Eqs. (A.2) and (A.7) is in fact a solution to the integral equation (A.1) only when $\tilde{\xi}$ lies outside the strip $|\text{Im}(\tilde{\xi})| \leq 1$.

The function $\tilde{\Phi}_0(\tilde{\xi})$ obtained above can be meromorphically extended into the strip $|\text{Im}(\tilde{\xi})| \leq 1$, however. For this purpose, notice that when the solution transform (A.2) is inserted into the integral of Eq. (A.1) and the resulting double integral is manipulated as above (see (A.3) and (A.4)), Eq. (A.1) then gives the following alternative expression for $\tilde{\Phi}_0(\tilde{\xi})$,

$$\tilde{\Phi}_0(\tilde{\xi}) = \frac{6}{1 + \tilde{\xi}^2} \int_{\mathcal{L}^\pm} \frac{1}{\sin^2 s} \phi(s) e^{-s\tilde{\xi}} ds, \quad (\text{A.10})$$

where $\phi(s)$ is given in Eq. (A.7). It is easy to see that the integral in (A.10) is convergent for all values of $\tilde{\xi}$ in the complex plane \mathbb{C} , thus the function $\tilde{\Phi}_0(\tilde{\xi})$ given by (A.10) is analytic for all $\tilde{\xi} \in \mathbb{C}$, save for the points $\tilde{\xi} = \pm i$ where it has simple-pole singularities. The two expressions (A.2) and (A.10) for $\tilde{\Phi}_0(\tilde{\xi})$ coincide when $\tilde{\xi}$ is outside the strip $|\text{Im}(\tilde{\xi})| \leq 1$, hence the function given by (A.10) also satisfies the integral equation (A.1) outside this strip. By taking the limit of $\text{Im}(\tilde{\xi}) \rightarrow \pm 1$, we can see that the function $\tilde{\Phi}_0(\tilde{\xi})$ given by (A.10) satisfies the integral equation (A.1) on the boundaries of this strip as well. Inside this strip, the function defined by (A.2) does not exist; hence, the solution to the integral equation (A.1) does not exist. Even though the function $\tilde{\Phi}_0(\tilde{\xi})$ given by the alternative expression (A.10) does exist inside this strip, this function does not satisfy the integral equation (A.1) in this region (this fact has also been confirmed by our numerical computations). When $\tilde{\xi} \rightarrow \infty$, the main contribution to the integral (A.2) comes from the vicinity of $s \sim 0$, and using the small- s asymptotics (A.8), we find that

$$\tilde{\Phi}_0(\tilde{\xi}) \rightarrow \frac{12C}{5} \frac{1}{\tilde{\xi}^4}, \quad \tilde{\xi} \rightarrow \infty. \quad (\text{A.11})$$

Appendix B. Numerical computation of recurrence relation

In this appendix, we outline the numerical procedure for solving the recurrence relation (3.15). We first write this recurrence relation as

$$\hat{L}_1 U_{n+2} = F_{n+2}(U_0, U_1, \dots, U_{n+1}), \quad n = 0, 1, 2, \dots, \quad (\text{B.1})$$

where

$$\hat{L}_1 = d^2/dx^2 + \mu_0 - V(x), \quad U_0 = p(x), \quad U_1 = iv(x), \quad (\text{B.2})$$

and

$$F_{n+2} = U_n - 2i \frac{dU_{n+1}}{dx} - \sigma a^2 \beta^2 \sum_{m=0}^n U_{n-m} \frac{(n-m)!}{(n+2)!} \\ \times \sum_{r=0}^m U_r U_{m-r} r! (m-r)!. \quad (\text{B.3})$$

Since $p(x)$ is a homogeneous solution of Eq. (B.1), the solvability condition of this inhomogeneous equation is then

$$\langle F_{n+2}(x), p(x) \rangle = 0, \quad (\text{B.4})$$

where the inner product is defined as

$$\langle f, g \rangle = \int_0^{2\pi} f(x)g(x)dx. \quad (\text{B.5})$$

When solving Eq. (B.1) itself, its solution U_{n+2} is not unique since it can contain an arbitrary homogeneous term $\zeta p(x)$, where ζ is a free constant. However, as shown below, the solvability conditions for later equations will uniquely determine U_{n+2} , and all solutions from this recurrence relation are unique.

We start with the solution U_2 which solves the equation

$$\hat{L}_1 U_2 = U_0 - 2i \frac{dU_1}{dx} - \frac{1}{2} \sigma a^2 \beta^2 U_0^3 \\ = p(x) + 2v'(x) - \frac{1}{2} \sigma a^2 \beta^2 p^3(x). \quad (\text{B.6})$$

The solvability condition for this equation is satisfied due to Eqs. (2.15) and (3.28), hence its solution is

$$U_2(x) = \hat{U}_2(x) + \zeta_2 p(x), \quad (\text{B.7})$$

where $\hat{U}_2(x)$ is a particular solution of Eq. (B.6), and ζ_2 is a real constant which is to be determined.

The recurrence equation for U_3 is

$$\hat{L}_1 U_3 = U_1 - 2i \frac{d\hat{U}_2}{dx} - \frac{1}{2} \sigma a^2 \beta^2 U_0^2 U_1 - 2i\zeta_2 p'(x). \quad (\text{B.8})$$

Recalling Eqs. (2.10) and (B.2) and performing integration by parts, the solvability condition for this equation becomes

$$0 = \langle v - \frac{1}{2} \sigma a^2 \beta^2 p^2 v, p \rangle + \langle \hat{U}_2, 2p_x \rangle \\ = \langle v - \frac{1}{2} \sigma a^2 \beta^2 p^2 v, p \rangle - \langle \hat{U}_2, \hat{L}_1 v \rangle \\ = \langle v, p - \frac{1}{2} \sigma a^2 \beta^2 p^3 - \hat{L}_1 \hat{U}_2 \rangle. \quad (\text{B.9})$$

Since \hat{U}_2 solves Eq. (B.6), the right-hand side of the above equation becomes $\langle v, -2v' \rangle$, which is obviously zero. Thus the solvability condition for Eq. (B.8) is automatically satisfied. Consequently, this equation is solvable, and its solution can be written as

$$U_3(x) = \hat{U}_3(x) + i\zeta_2 v(x) + i\zeta_3 p(x), \quad (\text{B.10})$$

where $\hat{U}_3(x)$ is a particular solution of Eq. (B.8) without the ζ_2 term, and ζ_3 is a new real constant.

The recurrence equation for U_4 is

$$\hat{L}_1 U_4 = U_2 - 2i \frac{d}{dx} (\hat{U}_3 + i\zeta_2 v) \\ - \frac{1}{8} \sigma a^2 \beta^2 (2U_0^2 U_2 + U_0 U_1^2) + 2\zeta_3 p'(x). \quad (\text{B.11})$$

Utilizing the solutions U_0, U_1 and U_2 in Eqs. (B.2) and (B.7), the solvability condition for the above equation gives

$$\zeta_2 \langle p + 2v' - \frac{1}{4} \sigma a^2 \beta^2 p^3, p \rangle \\ = -\langle \hat{U}_2 - 2i\hat{U}_3 - \frac{1}{8} \sigma a^2 \beta^2 (2p^2 \hat{U}_2 - pv^2), p \rangle. \quad (\text{B.12})$$

In view of Eqs. (2.15) and (3.28), the inner product on the left side of this condition is non-zero, thus this condition uniquely determines the value of ζ_2 ; hence, U_2 is now uniquely obtained. Since the

solvability condition for Eq. (B.11) is now met by the above choice of ζ_2 , the solution U_4 is then

$$U_4(x) = \widehat{U}_4(x) - \zeta_3 v(x) + \zeta_4 p(x), \quad (\text{B.13})$$

where $\widehat{U}_4(x)$ is a particular solution of Eq. (B.11) without the ζ_3 term, and ζ_4 is a new real constant. Utilizing this solution and imposing the solvability condition on the equation for U_5 , the constant ζ_3 in the solution U_3 would be uniquely determined as well.

The above procedure can be repeated for higher terms in the recurrence relation. Specifically, the coefficient ζ_{n+2} of the homogeneous term $p(x)$ in the solution U_{n+2} is determined by the solvability condition for the equation governing U_{n+4} . In this way, all solutions in the recurrence equation are unique and can be successively obtained.

As a numerical issue, we solved the linear inhomogeneous equations (such as (B.6) and (B.8)) by the preconditioned conjugate-gradient method [36]. Also, for convenience, we worked with the normalized variables $W_n = 2^n U_n$ so that the solutions do not decay quickly for large n .

References

- [1] D.N. Christodoulides, F. Lederer, Y. Silberberg, Discretizing light behaviour in linear and nonlinear waveguide lattices, *Nature* 424 (2003) 817.
- [2] Y.S. Kivshar, G.P. Agrawal, *Optical Solitons: From Fibers to Photonic Crystals*, Academic Press, San Diego, 2003.
- [3] O. Morsch, M.K. Oberthaler, Dynamics of Bose–Einstein condensates in optical lattices, *Rev. Modern Phys.* 78 (2006) 179.
- [4] in: P.G. Kevrekidis, D.J. Frantzeskakis, R. Carretero-Gonzalez (Eds.), *Emergent Nonlinear Phenomena in Bose–Einstein Condensates*, Springer, New York, 2008.
- [5] M. Skorobogatiy, J. Yang, *Fundamentals of Photonic Crystal Guiding*, Cambridge University Press, Cambridge, 2009.
- [6] J. Yang, *Nonlinear Waves in Integrable and Nonintegrable Systems*, SIAM, Philadelphia, 2010.
- [7] H. Eisenberg, Y. Silberberg, R. Morandotti, A. Boyd, J. Aitchison, Discrete spatial optical solitons in waveguide arrays, *Phys. Rev. Lett.* 81 (1998) 3383–3386.
- [8] D. Neshev, E. Ostrovskaya, Y. Kivshar, W. Krolikowski, Spatial solitons in optically induced gratings, *Opt. Lett.* 28 (2003) 710.
- [9] N.K. Efremidis, D.N. Christodoulides, Lattice solitons in Bose–Einstein condensates, *Phys. Rev. A* 67 (2003) 063608.
- [10] D.E. Pelinovsky, A.A. Sukhorukov, Y.S. Kivshar, Bifurcations and stability of gap solitons in periodic potentials, *Phys. Rev. E* 70 (2004) 036618.
- [11] B. Eiermann, Th. Anker, M. Albiez, M. Taglieber, P. Treutlein, K.P. Marzlin, M.K. Oberthaler, Bright Bose–Einstein gap solitons of atoms with repulsive interaction, *Phys. Rev. Lett.* 92 (2004) 230401.
- [12] J.W. Fleischer, M. Segev, N.K. Efremidis, D.N. Christodoulides, Observation of two-dimensional discrete solitons in optically induced nonlinear photonic lattices, *Nature* 422 (2003) 147–150.
- [13] C. Lou, X. Wang, J. Xu, Z. Chen, J. Yang, Nonlinear spectrum reshaping and gap-soliton-train trapping in optically induced photonic structures, *Phys. Rev. Lett.* 98 (2007) 213903.
- [14] R. Fischer, D. Trager, D.N. Neshev, A.A. Sukhorukov, W. Krolikowski, C. Denz, Y.S. Kivshar, Reduced-symmetry two-dimensional solitons in photonic lattices, *Phys. Rev. Lett.* 96 (2006) 023905.
- [15] G. Bartal, O. Manela, O. Cohen, J.W. Fleischer, M. Segev, Observation of second-band vortex solitons in 2D photonic lattices, *Phys. Rev. Lett.* 95 (2005) 053904.
- [16] Z. Shi, J. Yang, Solitary waves bifurcated from Bloch-band edges in two-dimensional periodic media, *Phys. Rev. E* 75 (2007) 056602.
- [17] J. Yang, Z. Musslimani, Fundamental and vortex solitons in a two-dimensional optical lattice, *Opt. Lett.* 28 (2003) 2094.
- [18] B.B. Baizakov, B.A. Malomed, M. Salerno, Multidimensional solitons in periodic potentials, *Europhys. Lett.* 63 (2003) 642.
- [19] D.N. Neshev, T.J. Alexander, E.A. Ostrovskaya, Y.S. Kivshar, H. Martin, I. Makasyuk, Z. Chen, Observation of discrete vortex solitons in optically induced photonic lattices, *Phys. Rev. Lett.* 92 (2004) 123903.
- [20] J.W. Fleischer, G. Bartal, O. Cohen, O. Manela, M. Segev, J. Hudock, D.N. Christodoulides, Observation of vortex-ring discrete solitons in 2D photonic lattices, *Phys. Rev. Lett.* 92 (2004) 123904.
- [21] E.A. Ostrovskaya, Y.S. Kivshar, Matter-wave gap vortices in optical lattices, *Phys. Rev. Lett.* 93 (2004) 160405.
- [22] H. Sakaguchi, B.A. Malomed, Two-dimensional loosely and tightly bound solitons in optical lattices and inverted traps, *J. Phys. B: At. Mol. Opt. Phys.* 37 (2004) 2225.
- [23] J. Wang, J. Yang, Families of vortex solitons in periodic media, *Phys. Rev. A* 77 (2008) 033834.
- [24] D. Song, C. Lou, L. Tang, X. Wang, W. Li, X. Chen, K. Law, H. Susanto, P.G. Kevrekidis, J. Xu, Z. Chen, Self-trapping of optical vortices in waveguide lattices with self-defocusing nonlinearity, *Opt. Express* 16 (2008) 10110.
- [25] T. Anker, M. Albiez, R. Gati, S. Hunsmann, B. Eiermann, A. Trombettoni, M.K. Oberthaler, Nonlinear self-trapping of matter waves in periodic potentials, *Phys. Rev. Lett.* 94 (2005) 020403.
- [26] T.J. Alexander, E.A. Ostrovskaya, Yu.S. Kivshar, Self-trapped nonlinear matter waves in periodic potentials, *Phys. Rev. Lett.* 96 (2006) 040401.
- [27] J. Wang, J. Yang, T.J. Alexander, Y.S. Kivshar, Truncated-bloch-wave solitons in optical lattices, *Phys. Rev. A* 79 (2009) 043610.
- [28] T.R. Akylas, G. Hwang, J. Yang, From nonlocal gap solitary waves to bound states in periodic media (under preparation).
- [29] Z. Shi, J. Wang, Z. Chen, J. Yang, Linear instability of two-dimensional low-amplitude gap solitons near band edges in periodic media, *Phys. Rev. A* 78 (2008) 063812.
- [30] N.G. Vakhitov, A.A. Kolokolov, Stationary solutions of the wave equation in a medium with nonlinearity saturation, *Izv. Vyssh. Uchebn. Zaved. Radiofiz.* 16 (1973) 1020. *Radiophys. Quantum Electron.* 16 (1973) 783.
- [31] K. Staliunas, R. Herrero, G.J. de Valcárcel, Diffraction management and sub-diffractive solitons in periodically driven Bose–Einstein condensates, *Physica D* 238 (2009) 1326–1337.
- [32] J. Yang, C.F. Schreck, H. Noh, S. Liew, M.I. Guy, C.S. O'Hern, H. Cao, Photonic-band-gap effects in two-dimensional polycrystalline and amorphous structures, *Phys. Rev. A* 82 (2010) 053838.
- [33] M. Rechtsman, A. Szameit, F. Dreisow, M. Heinrich, R. Keil, S. Nolte, M. Segev, Band gaps in amorphous photonic lattices, in: *Quantum Electronics and Laser Science Conference, OSA Technical Digest, Optical Society of America, 2010*, paper QMG1.
- [34] T.S. Yang, T.R. Akylas, On asymmetric gravity-capillary solitary waves, *J. Fluid Mech.* 330 (1997) 215–232.
- [35] D.C. Calvo, T.S. Yang, T.R. Akylas, On the stability of solitary waves with decaying oscillatory tails, *Proc. R. Soc. Lond. Ser. A Math. Phys. Eng. Sci.* 456 (2000) 469–487.
- [36] J. Yang, Newton-conjugate gradient methods for solitary wave computations, *J. Comput. Phys.* 228 (2009) 7007–7024.